

UNIVERSITÄT POTSDAM (UP)

Institut für Physik und Astronomie

Leibniz-Institut für Astrophysik Potsdam (AIP)



Master of Science

**Studying the Sagittarius dwarf galaxy
within the Pristine survey**

Supervisor:

Dr. Else Starckenburg (AIP)

Dr. Anke Arentsen (AIP)

Co-supervisor:

Prof. Dr. Maria-Rosa Cioni (UP, AIP)

Candidate:

Sara Vitali

Registration number:

799224

11/12/2020

Abstract

Sagittarius is a small dwarf galaxy that has been captured in the Milky Way potential. Many stars have been stripped away from its original structure, and now they form long tidal streams that wrap around our Galaxy as Sagittarius is being inexorably dragged towards the centre of the Milky Way. Despite this inevitable destruction, the core of the dwarf galaxy is still visible as a clear stellar over-density, but its great distance and closeness to the Galactic centre have hampered detailed studies of its properties.

The Sagittarius galaxy is also an evident and compelling example of cosmic cannibalism, being currently disrupted by the tidal forces of the Milky Way but still preserving an informative chemical evolution history. Moreover, Sgr dSph can be regarded as a survivor of the repeated encounters with our galaxy and it is a unique test case for investigating the processes behind their merger.

In this thesis we study the Sagittarius Spheroidal Galaxy (Sgr dSph) focusing especially on its metallicity distribution. In particular, its metal-poor stars are not well studied yet, but they are extremely important as they can provide what can be regarded as “archaeological” evidences of the earliest times of the evolution of Sagittarius. Indeed, the research and study of the most metal-poor stars present in the galaxy can furnish clues about the dynamical history and its interaction with the Milky Way.

To enable a careful study of this population, we use data from the Pristine Inner Galaxy Survey (PIGS). This photometric survey is very metallicity sensitive and it is therefore able to select the most metal-poor populations in the Sagittarius galaxy. To gain a broader insight into the metallicity distribution of this satellite, we apply on four spectroscopic catalogues the Ca II triplet (CaT) technique, which is an empirical method that allows the derivation of the $[\text{Fe}/\text{H}]$ content using the strength of the CaT absorption lines. By combining the CaT results with the Pristine photometry and with the second spectroscopic release from the Apache Point Observatory Galactic Evolution Experiment (APOGEE), we collect metallicity information about Sagittarius, whose star members are selected thanks to the astrometric data provided by the Gaia DR2. In this way, we provide a more complete picture of the galaxy and compare the results about its core with the studies performed on the long stellar tails.

Especially, by focusing on its metallicity distribution, we find a pronounced metallicity gradient within the Sgr core. We study the spatial distribution of the most metal-rich and metal-poor selections derived thanks to the metallicity-sensitive photometry. By analysing the variation of their ratios in space, we conclude that the relative number of metal-poor stars is higher in the outer areas of the system.

With the investigation of the metallicity pattern in Sgr and by comparing the properties of the metal-poor and metal-rich components, we aim to better understand the

history and evolution of Sagittarius, adding insights on what the galaxy used to look like before its interaction with the Milky way.

Zusammenfassung

Die Sagittarius-Zwerggalaxie ist im Potential der Milchstraße gefangen. Viele Sterne sind aus der ursprünglichen Struktur gelöst worden und bilden lange Gezeitenströme. Diese umschlingen unsere Galaxie während sie sich unauflösbar dem Zentrum der Milchstraße nähert. Trotz seiner unausweichlichen Zerstörung, ist der Galaxien noch deutlich als stellare Überdichte zu erkennen, auch wenn seine große Entfernung von uns und seine Nähe zum Galaxiekern detaillierte Untersuchung seiner Eigenschaften verhindert haben.

In dieser Arbeit untersuchen wir die elliptische Sagittarius-Zwerggalaxie (Sgr dSph) mit einem Schwerpunkt auf der Verteilung der Metallizität. Insbesondere sind seine metallarmen Sterne noch nicht ausführlich untersucht, die jedoch überaus wichtig sind, da sie als archäologische Anhaltspunkte der frühesten Entwicklung von Sagittarius angesehen werden können. Tatsächlich kann die Untersuchung der metallärmsten Sterne dieser Galaxie Hinweise auf die dynamische Entwicklungsgeschichte und auf die Interaktion mit der Milchstraße geben.

Um eine genaue Untersuchung dieser Sternpopulation zu ermöglichen, nutzen wir die Daten des Pristine Inner Galaxy Survey (PIGS). Dieser Survey ist sehr empfindlich auf die Metallizität und daher geeignet die metallärmsten Sternpopulationen in der Sagittarius-Galaxie zu identifizieren. Um einen umfassenderen Einblick in die Metallizität des galaktischen Satelliten zu gewinnen, wenden wir die Ca-II-triplet-Methode (CaT) auf insgesamt vier Kataloge an. CaT ist eine empirische Methode, die Ableitung des $[\text{Fe}/\text{H}]$ -Betrages über die Absorptionsstärke der CaT Linien ermöglicht. Durch die Verbindung der CaT-Ergebnisse mit sowohl der Photometrie des Pristine Surveys als auch der zweiten Veröffentlichung des Apache Point Observatory Galactic Evolution Experiment (APOGEE), sammeln wir Information über Sagittarius, dessen Mitglieder wiederum durch die astrometrischen Daten von Gaia DR2 selektiert werden. Auf diesem Wege erreichen wir ein vollständigeres Bild der Galaxie und vergleichen zudem die Ergebnisse ihres Kerns mit Untersuchungen zu den stellaren Ausläufern.

Weiterhin illustriert Sagittarius deutlich den Prozess des kosmischen Kannibalismus. Sagittarius ist ein spannendes und offenkundiges Beispiel des kosmischen Kannibalismus, da sie von den Gezeitenkräften der Milchstraße auseinandergerissen wird und gleichzeitig ihre chemische Evolutionsgeschichte erhält.

Durch die Untersuchung von Sgr dSph im oben genannten Rahmen zielt die vorliegende Masterarbeit darauf ab, Sagittarius als berlebende mehrfacher Begegnungen mit der Milchstraße zu zeichnen und die zugrunde liegenden Abläufe ihrer Verschmelzung zu klären. Insbesondere ermöglicht der Schwerpunkt auf der Metallizitätsverteilung ein besseres Verständnis der Geschichte und Entwicklung von Sagittarius und erlaubt so weitere Einblicke in ihre Struktur vor der Begegnung mit der Milchstraße.

List of Acronyms

APOGEE Apache Point Observatory Galactic Evolution Experiment

PIGS Pristine Inner Galaxy Survey

Sgr dSph Sagittarius dwarf spheroidal galaxy

Sgr dE Sagittarius Dwarf Elliptical Galaxy

Sgr DEG Sagittarius Dwarf Elliptical Galaxy

ISM Interstellar medium

MW Milky Way

CaT Calcium Triplet

Contents

| | | |
|----------|--|-----------|
| 1 | Introduction | 1 |
| 1.1 | Definitions & Nomenclature | 1 |
| 1.1.1 | Abundance definition | 1 |
| 1.1.2 | Nomenclature | 1 |
| 1.2 | Galactic Archaeology | 2 |
| 1.3 | The importance of the metal-poor stars | 4 |
| 1.4 | Substructures and satellites | 6 |
| 1.5 | Pristine Survey and the first stars | 6 |
| 2 | The Sagittarius dwarf galaxy | 9 |
| 2.1 | An overview over Sagittarius Galaxy | 9 |
| 2.2 | Morphology | 10 |
| 2.2.1 | M54 | 12 |
| 2.3 | Sagittarius stellar streams | 13 |
| 2.4 | Orbit & Proper motion | 15 |
| 2.5 | Stellar populations in Sagittarius | 16 |
| 2.6 | Chemical composition | 18 |
| 3 | Data | 20 |
| 3.1 | PIGS Catalogue | 21 |

CONTENTS

| | | |
|----------|---|-----------|
| 3.2 | Sample selection | 22 |
| 3.3 | Extinction correction | 26 |
| 3.4 | Description and analysis of the available spectroscopic samples | 27 |
| 3.4.1 | PIGS follow-up | 27 |
| 3.4.2 | APOGEE catalogue | 28 |
| 3.4.3 | The CaT catalogues | 30 |
| 3.5 | Catalogues comparison | 36 |
| 4 | Results | 40 |
| 4.1 | Photometric selection | 40 |
| 4.1.1 | Proper motion analysis | 43 |
| 4.2 | Metallicity distribution | 46 |
| 4.2.1 | Concentric distribution | 47 |
| 4.2.2 | Elliptical distribution | 50 |
| 4.3 | Variation of the spatial density vs. metallicity | 51 |
| 4.3.1 | Insight on the VMP | 52 |
| 4.4 | Age of VMP stars in Sgr | 54 |
| 4.5 | Outline of the main findings | 56 |
| 5 | Discussion | 57 |
| 5.1 | Comparison with literature | 57 |
| 5.1.1 | Comparison with Fornax Dwarf Spheroidal Galaxy | 60 |
| 5.2 | Limitations of the research | 61 |
| 5.3 | Future outlook | 62 |
| 6 | Summary and conclusion | 65 |
| 7 | Bibliography | 67 |

CONTENTS

| | |
|-------------------|-----------|
| Appendices | 72 |
| Appendix A | 73 |

Chapter 1

Introduction

1.1 Definitions & Nomenclature

Before start to explore the main topic of this work which aims to guide the reader through the history and evolution of the unique system of Sagittarius, we would like to set the stage by giving some definitions and the nomenclature that will be used throughout the thesis.

1.1.1 Abundance definition

Usually the abundance of an element in a star is expressed in a logarithmic scale relative to the content of Hydrogen. For stars, the values are generally compared to the solar abundances. If we name the element A, we have:

$$[A/H] = \log_{10}(N_A/N_H)_\star - \log_{10}(N_A/N_H)_\odot \quad (1.1)$$

Since Iron shows the richest absorption lines in the optical spectral region, it is more convenient to measure this element than the other abundances, it is thus representative of the overall stellar metallicity. Taking Fe as element, the metallicity is expressed as:

$$[Fe/H] = \log_{10}(N_{Fe}/N_H)_\star - \log_{10}(N_{Fe}/N_H)_\odot \quad (1.2)$$

Hence, if a star has $[Fe/H] = -3$, this means that its iron abundance is 1/1000 of the solar one.

1.1.2 Nomenclature

In view of the previous definition, the metal-poor stars can be divided and classified according to their iron content following the nomenclature in table 1.1 (Beers

| Denomination | [Fe/H] | Fe relative to Sun |
|----------------------------|--------|--------------------|
| Metal-poor (MP) | < -1 | 10^{-1} |
| Very metal-poor (VMP) | < -2 | 10^{-2} |
| Extremely metal-poor (EMP) | < -3 | 10^{-3} |
| Ultra metal-poor (UMP) | < -4 | 10^{-4} |
| Hyper metal-poor (HMP) | < -5 | 10^{-5} |
| Mega metal-poor (MMP) | < -6 | 10^{-6} |

Table 1.1 – *Classification of metal-poor stars.*

& Christlieb, 2005). These different types of stars have differences not only in term of iron content, but also regarding the stellar populations and chemical properties. A detailed classification of the metal-poor stars is presented by Beers & Christlieb, 2005. The division in different populations is based on the metallicity content of the stars. It was introduced in the '40s by the astronomer W.H.W. Baade. He realized that there are two types of stars in the galaxy, the stars belonging to Population I, which are brighter and closer, while the fainter and more distant ones are part of Population II. The members of the first group show properties similar to the solar ones, they are younger than 10 billion years and they can be both recently formed and forming stars. They are metal-rich in having 2% to 3 % heavy elements (Kurucz et al., 1992), while the rest is composed of Hydrogen and Helium. They are constrained in the disk region and in dusty areas favourable to star formation. The Population II is made up of older stars with an age of over 10 billions years (Kurucz et al., 1992). They are metal-poor, being composed of less than 0.1 % metals. The location of this stellar group is usually the galactic halo, but they can also be found in globular clusters or in the central bulge. Also the kinematic properties are very different (i.e. orbits and motions). A third class, Population III, exists incorporating the primordial stars, that is the stars composed almost entirely of Hydrogen and Helium. This last category will be discussed in more details in the next sections due to its relevance in the field of Galactic Archaeology and in the study of the evolution of our Galaxy.

1.2 Galactic Archaeology

As the archaeologists try to reconstruct the history of our world, astronomers, with large telescopes and surveys, attempt to find the messengers of the earliest Universe in the Galaxy. This type of research is recognised to be a part of a broad and extremely fascinating scientific field: Galactic Archaeology. This discipline examines stellar “records” in order to draft the history of our nearby Universe. Its name evokes a science that is aimed to the study the past, where in this context the past is the earliest time of the Universe that can be investigated through the remnants observable

today. These observables are the descendants of the very first stars (belonging to the Population III) that formed from a zero metallicity gas: pristine gas.

Immediately after the Big Bang, the composition of the Universe was quite simple: as the Universe expanded and cooled down within a few minutes from its formation, the first light elements formed. These were mainly Hydrogen ($\sim 75\%$), Helium ($\sim 25\%$), small traces of Deuterium ($\sim 0.01\%$) and Lithium (in the order of $\sim 10^{-10}$) (Frebel & Norris, 2011). The pristine gas is the remnant of this primordial composition.

Today, in a Universe aged ~ 13.8 Gyr, stars with very low abundance of metals are a precious medium to get an idea about the origin of the elements that were recycled during the history of the Universe and that have polluted the medium where all the last generations of stars have been born. Indeed, these stellar records correspond to an insight in the high-redshifted Universe. In the mid-twentieth century, it was discovered and generally accepted that stars show a wide range of chemical features and especially several metallicities. In this vast and populated landscape of chemical properties, the galactic archaeology field has the aim of the research of the first stars, whose formation is still object of debates and discussions.

It was 1981 when the American astronomer Bond wondered about the possibility to observe and locate the stars belonging to Population III. Before this date, no stars with $[\text{Fe}/\text{H}] < 1/1000$ were discovered (Frebel & Norris, 2011). It took another three years before the first star with $[\text{Fe}/\text{H}] = -4.5$ was revealed by Bessell & Norris (1984) and named CD $-38^\circ 245$. This star had maintained the primacy as the lowest metallicity target until it was discovered that the real metal content was ~ -4.0 (Norris et al. 2001). In the course of the years, with the development of the search techniques, the metallicity limits have considerably decreased as it can be seen in fig. 1.1.

So far, the most metal-poor stars observed are found to have $[\text{Fe}/\text{H}]$ around -6 , e.g. $[\text{Fe}/\text{H}] < -6.53$ (Nordlander et al., 2017) and $[\text{Fe}/\text{H}] < -6.1$ (Aguado et al., 2019). Among the most metal-poor stars sticks out SMSS J03136708, whose discovery was announced by Keller et al. (2014). This object, showing an iron content of $[\text{Fe}/\text{H}] \leq -7.1$ is seen as a precious proof of the first stars belonging to Population II.

How essential and captivating this research is thought to be, the detection of these old and metal-poor stars is at the same time very challenging: Hartwick in 1976 formulated a model for the halo chemical enrichment (under the assumption that the halo has originally no heavy-elements) which states that the number of stars decrease with iron abundance: from $[\text{Fe}/\text{H}] < -1.5$ to $[\text{Fe}/\text{H}] < -3.5$ there is a drop by a factor of 100.

Many recent studies (Schörck et al., 2009) have agreed on the rareness of these MP objects. Youakim et al. (2017) showed that (considering an halo stellar metallicity distribution peaking at $[\text{Fe}/\text{H}] = -1.5$) it is possible to detect in the solar neighbourhood (but looking towards the halo) only 1 in ~ 800 stars with $[\text{Fe}/\text{H}] < -3$. If we go down to even lower metallicities, there are just a few examples: nowadays, just ~ 40 stars have been discovered with $[\text{Fe}/\text{H}] < -4$.

possible today to observe the stars belonging to population III.

The major mechanisms responsible for the enrichment of the ISM are the Supernovae explosions which are divided in two major categories: Type Ia (SN Ia) and Type II (SN II). The formation of the first type is generally linked to a binary system in which one of the two body is a carbon-oxygen white dwarf. The white dwarf accretes mass from its companion reaching a mass limit beyond which a nuclear fusion reaction sets and leads to the Supernova explosion. This process mainly produces iron. On the other hand, the SN II creates mostly the so-called α -elements, such as magnesium, neon, silicium, argon, calcium, sulfur. They originate from the sudden collapse of a very massive stars that triggers the explosion and the ejection of the outer layers.

As already mentioned before the first stars must have been extremely massive, nevertheless the metal-poor stars observed today are low-masses objects ($\lesssim 1M_{\odot}$, De Boer) mostly main-sequence and giant stars (Frebel & Norris, 2011). The major process responsible for the gas fragmentation that then allows the formation of smaller stars is the fine-structure line cooling by C and O nuclei (Bromm, 2013). In this case, radiative processes of the atoms, ions, or molecules release kinetic energy into radiation after being excited by collisions. The most efficient ions and atoms that allow this cooling mechanism are the ones that have fine-structure levels and thus they are easy to be excited. In the ISM these are primarily C II and O I. These elements cause the temperature to diminish creating the conditions (dense and cool gas) for low-mass stars to form. Observations indicate that the coldest clouds tend to form low-mass stars, that are first observed in the infrared from inside the clouds and then in visible light at their surface when the clouds dissipate. The passage from the third to the second population is caused by the dust grains that come from the SNe explosions and which lead to the creation of sub-solar structures.

The idea that the most MP stars can be considered messengers from the early Universe is valid if they are also among the oldest stars ¹. It is generally found that this is the case: the most MP stars in the Galaxy are older than the average and vice versa (Starkenburg et al., 2017). By using cosmological simulations, Starkenburg et al. (2017) showed that in a typical Milky Way galaxy the older and more MP stars are usually found at the outskirts of the galaxy. Nevertheless, if the observer is able to overcome the difficulties that concern the observation of the centre of a galaxy, the probability of finding stars that are both old (even stars formed before the reionization epoch) and MP (at the same time) is higher.

Focusing the attention on Sagittarius, it is interesting to compare its metallicity distribution with the the one of our galaxy and investigate whether they share the same metallicity distributions or not, so to be able to understand its history and evolution.

¹That is their formations should have occurred around formation < 0.8 Gyr after the Big Bang. The choice of this value, which corresponds to a redshift $z > 6.9$, is justified in the paper Starkenburg et al. (2017). Indeed by setting $z = 6.9$, they constrain the formation of the oldest stars close to the reionization epoch.

1.4 Substructures and satellites

The variety of galaxies present in the Universe, with their different shapes, features, and sizes demonstrates the existence of numerous formation processes behind these galactic structures. The driving force responsible for this clustered and dense panorama is thought to be Gravity. Starting from small over-dense regions, their mutual attractions led to the assembly of larger structures such as our Galaxy. The higher density fluctuations that crossed the Early Universe created the building blocks of the galaxies which then merged together and are possible locations of the oldest stars (Helmi et al., 2006).

Some of the mergers are still going on today, and the Sagittarius dwarf galaxy, being disrupted by the tidal forces of the Milky Way, is an illustrative example of the “cosmic cannibalism” process. This term refers to events in which smaller galaxies are devoured by larger and bigger ones. Most of the outer halos of galaxies are thought to be the results of these mergers, as they are built up from the debris of the smaller systems (De Lucia & Helmi, 2008). The first parts of the devoured galaxies to be stripped away are the outers ones, being easier to be unbound. These disruptive processes are part of the big scenario of the hierarchical clustering (or hierarchical merging). This process involves the growth in size of the bigger structures via the merging with lower-mass objects. Nevertheless, it is possible that some of the “cannibalized” objects preserve their identities and turn into satellites orbiting around the main larger body for a long period of time. The dwarf galaxies, orbiting as satellites around the Milky way, which are still observable today can be regarded as what is left of these merging processes. They have survived across time and preserve information about their prolonged star formation and chemical evolution histories. Hence, the Milky Way and its satellites constitute a good example for studying the still unclear physical mechanisms that affect its star formation history, and shed a light on the early interactions and star formation processes involved in our Galaxy.

1.5 Pristine Survey and the first stars

Finding the most MP stars is the main concern of the Pristine survey that started taking data in 2015 and was first presented later in 2017 (Starkenburg et al., 2017). Pristine is a narrow-band survey covering a region of $\sim 5000 \text{ deg}^2$. It operates mainly in the Northern hemisphere looking at galactic latitude with $30^\circ < b < 73^\circ$ plus a small region at lower declination that is part of the bulge and the Sgr survey. Pristine focuses on the research and study of the most metal-poor stars around the Local Group, an astronomical field that has been greatly developed in the last decades as it is proved by the number (~ 13) of stars discovered with $[\text{Fe}/\text{H}] < -4.5$ (Starkenburg et al., 2017)).

Pristine has a different approach than the main spectroscopic surveys (as SDSS,

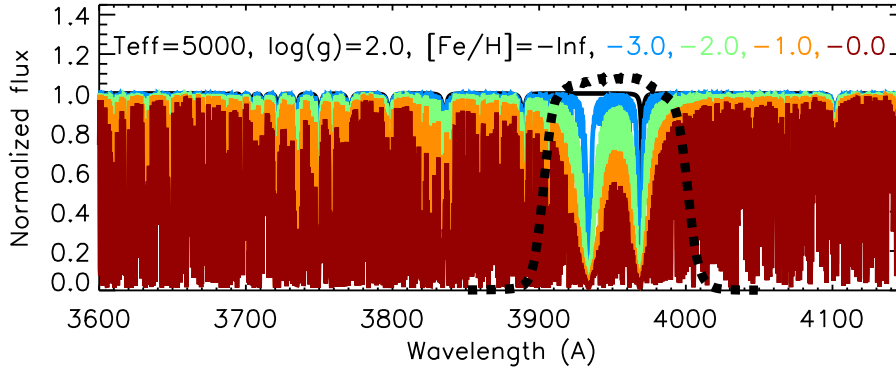


Figure 1.2 – *Ca II H & K filter put on top of synthetic spectra of stars of different metallicities. It is possible to see that the absorption lines become narrower and narrower with decreasing in metallicity. Courtesy: E. Starkenburg*

SEGUE, and LAMOST). It makes use of a special and innovative hardware: the narrow-band Ca H&K filter designed for the MegaCam wide-filter imager, mounted on the 3.6-m Canada-France-Hawaii Telescope. This narrow-band filter is devised to look at a particular spectral region of the blue optical wavelengths where we find the Ca II H & K absorptions lines (corresponding to 3969 and 3933 Å). These lines had been already employed in the past by the Hamburg/ESO (HES) HK survey (Christlieb et al., 2008)). The idea behind is to use these absorption lines to separate the MP from the MR stars, as the lines constitute a good proxy since a MP star shows weaker Ca H&K lines, which become narrower and narrower going down to lower metallicities. Indeed, for two stars of different metallicities but with the same temperature it is possible to distinguish a MP-star from a MR-one by comparing their absorption lines. Therefore, these spectral features are really good indicators of the metallicity of a star and thus they have been chosen as targets of the Pristine filter shown in fig 1.2. It covers a region $\sim 100\text{\AA}$ wide containing the two Ca H&K lines. Its narrowness and top-hat-shape makes it less likely to be influenced by the molecular bands of C and N enhanced stars.

In combination with the SDSS broad-band g and i photometry, the SDSS- Pristine colour-colour space was created (Starkenburg et al., 2017) and it enables to obtain a clear spread for different metallicity values, see fig. 1.3. Its sensitivity to the metallicity is restricted to a temperature range that goes from the turn-off (in hotter stars ionization processes take over and H lines become dominant) to the tip of the red giant branch (in cooler objects the molecular bands dominate the stellar spectra).

Fig.1.3 gives an idea of the resulting conversion from the Ca H&K magnitudes to a photometric metallicity scale. Starkenburg et al. tested the possibility to infer the $[\text{Fe}/\text{H}]$ values thanks to the photometric metallicity scale and found that this could be done for a range from $[\text{Fe}/\text{H}] = -0.5$ to $[\text{Fe}/\text{H}] = -3.0$ (with a precision of ~ 0.2 dex). The Pristine Survey has thus enabled to reach values of metallicity that were not possible to study until now without the aid of spectroscopy. The fact that no pre-selection is needed for simultaneously measuring all the stars in a field of view is a clear advantage of this technique. Moreover, the filter is less sensitive (especially in

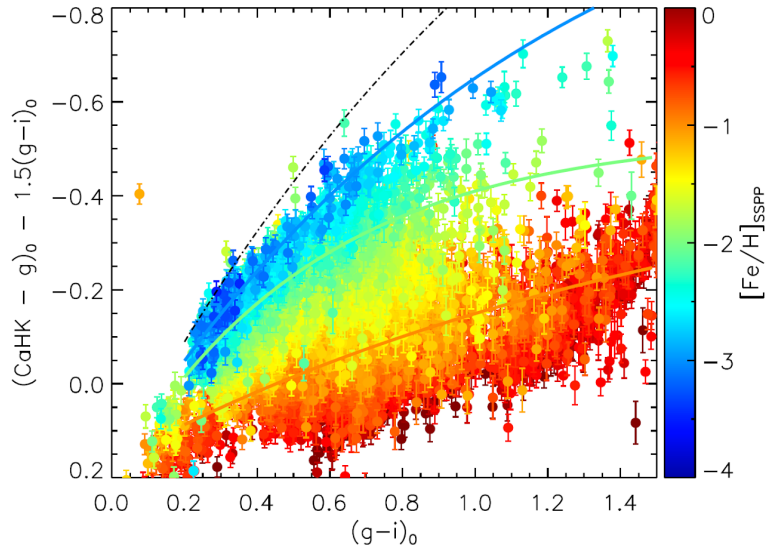


Figure 1.3 – *Photometric selection of metal-poor stars using the Ca H&K filter in combination with SDSS broad-band photometry. Courtesy: Starkenburg et al..*

the metal-poor regime) to some stellar parameter, as surface gravity, with respect to temperature and metallicity and this makes it very metallicity-selective (Starkenburg et al., 2010). The effectiveness of the narrow-band photometry is fully proven by the growth of a factor of five (Youakim et al., 2017) in efficiency in the search of EMP stars compared to the previous surveys operating in the same field .

Covering also the faint dwarf galaxies in the Northern hemisphere, the Pristine photometry is a precious tool to isolate the member stars of dwarf galaxies. It operates on faint stars for which spectroscopy is not really effective and helps to obtain a clean sample from the halo contamination of the members belonging to the dwarf galaxies. This is also the case for Sagittarius galaxy, which is part of the Pristine footprint.

Chapter 2

The Sagittarius dwarf galaxy

2.1 An overview over Sagittarius Galaxy

The Sagittarius Dwarf Spheroidal Galaxy (Sgr dSph) is an elliptical satellite galaxy of the Milky Way (MW). It can boast of being the nearest massive dwarf galaxy of the Milky Way. Its distance modulus is $(m - M)_0 = 17.10$ (Ferguson & Strigari, 2020) which corresponds to an heliocentric distance of $D = 26.41$ kpc. It is oriented perpendicular to the plane of the Galaxy.

It was discovered in 1994 by Ibata, Gilmore and Irwin (Ibata et al., 1994), when a large group of comoving stars (as shown in fig.2.1) was detected looking in the direction of the constellation of Sagittarius. The astronomers named it Sagittarius dwarf galaxy, being located in the constellation of Sagittarius. Its properties and features were recognised to be comparable with those of the other dwarf galaxies orbiting around the Milky Way. Being located on the other side of the Galactic centre (fig.2.2), the observation of Sagittarius is highly difficult due to the dust and the large number of foreground and background stars. Looking in the direction of Sgr ($l \sim 5^\circ$ and $b \sim -14^\circ$), it is necessary to consider the contamination from different galactic populations: the Milky Way bulge, acting on a distance of $\sim 6 - 10$ kpc, and the thin and thick disk stars, respectively up to ~ 2 kpc and ~ 6 kpc (Ibata et al., 1996). During the first observations, the field of view was restricted, nevertheless, it was immediately recognised that Sgr shows a tidally disrupted elongated structure that crosses a remarkable portion of the celestial sphere. Despite the difficulties due to its position, Sgr is one among the most investigated halo substructure, being a compelling example of enduring interaction with the MW.

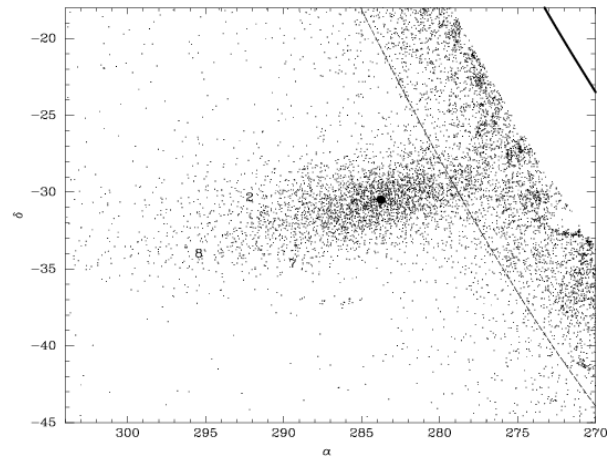


Figure 2.1 – *Sgr dSph*. The galaxy was discovered by Ibata et al. in 1994. The continuous black line marks the division with the Milky way bulge, situated at the top right. Courtesy: Ibata et al. (1994, *Nature*)(Ibata et al., 1994)

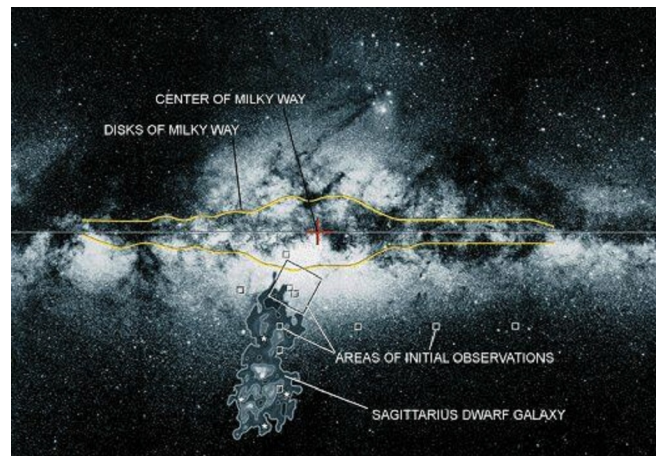


Figure 2.2 – *Sagittarius galaxy interacting with the Milky Way*. Courtesy: (Ibata, Wyse, Gilmore, Irwin & Suntzeff, *Sgr*).

2.2 Morphology

Despite its irregular shape, Sgr is defined as a dwarf spheroidal galaxy since no HI observations has been detected in the galaxy (Majewski et al., 2003). In fact, these are features of the rotational curves which are usually found for spiral galaxies. It hosts both old and younger stars which are proofs of several star formation episodes (Sarajedini & Layden, 1995) and since it is depleted in gas as a typical spheroidal galaxy, there is no on going star formation. Another denomination for Sagittarius is Dwarf Elliptical Galaxy (Sag DEG, Sgr dE) because of its irregular an prolate shape and due to a protracted star formation history, which is a feature shared also by Local

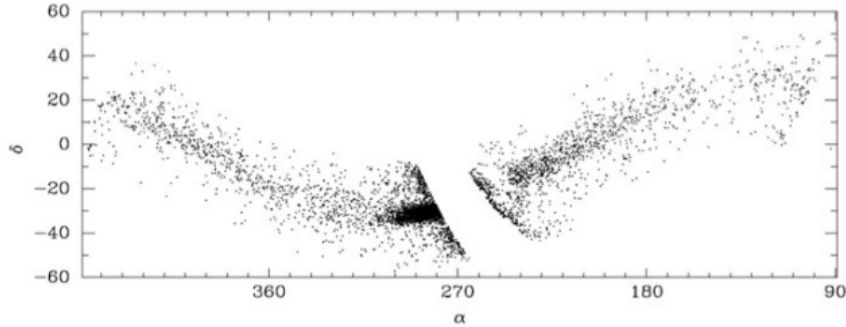


Figure 2.3 – Tracks in equatorial coordinates of Sgr stellar streams derived by the sample of bright M giants observed within the 2MASS survey (Majewski et al., 2003).

Group dwarf elliptical galaxies (dE) (Freeman, 1993). Indeed, the three-dimensional shape presented by Ibata et al. as a “prolate spheroid” has been recently confirmed by del Pino et al. (2020). By combing *Gaia* DR2 data and machine learning techniques, they validated the idea that Sgr has a prolate shape that can be described as a triaxial ellipsoid whose major axis (~ 3 kpc) is inclined $\sim 43^\circ$ with respect to the plane of the Sky and the axes ratios are 1:0.67:0.60. This moulded shape is the result of the MW tidal forces exerted on the dwarf system. The inner (or bulk) region still preserves a nucleus extended for 500-330-300 pc that has a clock-wise rotation of about 4.13 km s^{-1} around its intermediate axis (del Pino et al., 2020).

The amount of dark matter in Sgr is still under a controversial debate. Only some time after the Sgr discovery, the mass to light ratio was presented as $M/L_v \sim 50$ (Ibata et al., 1996). A constant-density dark halo model was adopted to describe the system. At that time it was thought that the galaxy could not be much larger than observed, since the missing mass lost by the original system and then transferred in the tidal debris tails was found years later. An extremely complete mapping of the streams was performed by Majewski et al. (2003) who, using the positions of the bright M giants provided by the 2MASS survey, plotted the Sgr streams onto a wide all-sky view, as represented in fig.2.3. After some time, it was evident that Sagittarius was going under a tidal disruption and assimilation process into the Milky Way Galaxy (Ibata, 1999). This scenario put a new constrain on the dark matter content of the galaxy, leading to $M_\odot/L_\odot \sim 100$, (Ibata et al., 2001). This value should have explained the survival of Sgr in its orbit despite the repeated mass-loss events during its path around the Galaxy. More recent studies, e.g. Majewski et al., testing and comparing different profiles for the Sgr main body presented new results: $M_\odot/L_\odot \sim 25 - 29$ with the mass value ranging from $4.9 \times 10^8 M_\odot$ to $5.8 \times 10^8 M_\odot$. The mass of the main body of Sgr, or also called Sgr “nucleus” is estimated to be around $\sim 2 \times 10^7 M_\odot$ (Mucciarelli et al., 2017). The big difference between the previous values is due to the different parameters adopted in the models representing the system and elected limits for the bound Sgr mass. In fact, today, thanks to the astrometric and photometric data of *Gaia* Data

Release 2, it is possible to construct a very clean selection of the Sgr members from the MW foreground. By taking advantage of this possibility, Vasiliev & Belokurov (2020) performed a N-body simulation for analysing the disruption of Sgr as it orbits the MW. They concluded that the remaining mass of Sgr is $\sim 4 \times 10^8 M_{\odot}$ with just a quarter in stellar content. Additionally, they predicted that Sgr galaxy will inexorably dissolve over the next Gyr, a period of time that coincides with its next orbit. There is still debate as del Pino et al. foresee that Sgr will survive the last pericenter passage and won't be disrupted in its totality.

2.2.1 M54

The brighter globular cluster (GC) which resides at the centre of the Sgr main body is known as Messier 54 or NGC 6715. Its coordinates are $\alpha \simeq 18.55^{\circ}$ and $\delta \simeq -30.28^{\circ}$ (Harris catalogue). Together with M54, Sgr hosts other globular clusters: Terzan7, Terzan8, Arp 2 and Palomar 12.

M54 has been presented as the most metal-poor ($[\text{Fe}/\text{H}] \lesssim -1.5$) and oldest part (~ 13 Gyr) of Sgr galaxy itself (Sarajedini & Layden, 1995). Its mass is about $2 \times 10^6 M_{\odot}$ (Mackey & Gilmore, 2003). Moreover, M54 with its larger metallicity span $\Delta[\text{Fe}/\text{H}] \sim 0.16$ (Bellazzini et al., 2008) departs from the "classical" GCs that generally show $\Delta[\text{Fe}/\text{H}] \sim 0.05$ dex (Carretta et al., 2009). This metallicity range has been connected to the presence of different stellar populations. Indeed, Alfaro-Cuello et al. (2019) detected a young metal rich, an intermediate-age metal rich and a old metal poor populations residing in M54.

Being at the same distance of Sgr, ~ 27 kpc and showing similarity in radial velocities ($\sim 140 \text{ Kms}^{-1}$), the GC has been for long time identified as the nucleus of the dwarf galaxy (Sarajedini & Layden, 1995). However, during the years contrary opinions emerged e.g. Bellazzini et al. (2008) and asserted that the nucleus of Sgr had formed independently from M54 and then it was dragged into the centre of the galaxy due to decay of the original orbit. As a matter of fact, M54 appears much brighter with $M_V \sim -10$ (Simbad database) in comparison with the surrounding Sgr field stars. It was also shown by Da Costa & Armandroff (1995) that the integrated colour of M54 is bluer compared to that of Sgr. Another difference concerns the metallicity content, in fact the nucleus of Sgr should be at least as metal-rich as the surrounding but M54 is more metal-poor. In 2008, Bellazzini et al. advanced the idea that the Sgr nucleus (also called "Sgr,N") formed completely independent from M54. A strong density enhancement was detected which peaks exactly where M54 resides. They demonstrated that the Sgr galaxy has a nucleus of metal-rich stars whose centre corresponds to the one of the GC which could have fallen into the potential well of Sgr galaxy overlapping with the central overdensity. Therefore, Sgr,N and M54 share the same position and radial velocity due to an important orbital decay of this latter that was induced by dynamical friction. Nevertheless, they constitute two different systems: M54 is a baryonic self-gravitating GC, while Sgr dSph is dark matter-dominated. Another possibility (Bellazzini et al., 2008) is that M54 was born *in situ*, created from Sgr gas



Figure 2.4 – *M54 or NGC 6715. Courtesy: Wide Field Channel of Hubbles Advanced Camera for Survey.*

and then, after falling to the bottom of the potential well, it attracted the Sgr stars from the surrounding.

Despite the uncertainty about the origin of M54, Sgr is eventually considered a nucleated dwarf galaxy since it shows a resolved central nucleus, even ignoring the presence of M54 (Bellazzini et al., 2008). Hence, a nucleus formed by the Sgr stars lie in the same region of the GC but it does not belong to M54.

2.3 Sagittarius stellar streams

Sagittarius could be considered before the in-fall as one among the most massive galaxy around the Milky way (McConnachie, 2012) - following the Large and Small Magellanic Clouds - with a mass of $\sim 10^8 M_{\odot}$ and a total luminosity in the range of $10 - 14 L_{\odot}$, where the core contribution is $2.4 \cdot 10^7 L_{\odot}$ while the stream luminosity is between $7 - 9 \cdot 10^7 L_{\odot}$ (Newberg & Carlin, 2015).

Sgr has shed a large percentage of its initial mass due to the interaction with the Milky Way. It has lost roughly half of its stars (Newberg & Carlin, 2015), reducing its initial mass-to-light ratio from $\Upsilon_{\odot} = 100$ to $\Upsilon_{\odot} = 5 - 25$.

It is again the interaction with the Milky Way that is responsible for the extended tidal tails (leading and trailing arms) which help us to track the path of Sgr through the Milky Way. Both the leading and trailing streams are formed from the tidally disrupted stars that have been removed during the long interaction history between Sgr and the MW and they are now arranged in long wrapping streams that do more than a complete revolution of the sky. The two tails cross M54. They are displayed in fig.2.5 and 2.6, which have been created with the simulation files from the Law & Majewski

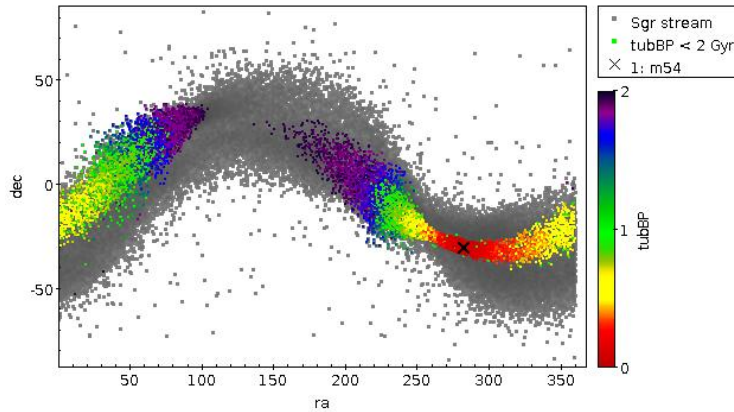


Figure 2.5 – The figure shows the leading and trailing streams in spatial coordinates. Both pass through the Sgr main body overdensity located at $\alpha \sim 283^\circ$ and $\delta \sim -30^\circ$. The colour-coded points represent the stars that have been recently unbound - in a range of time of 2 Gyr - from the Galaxy.

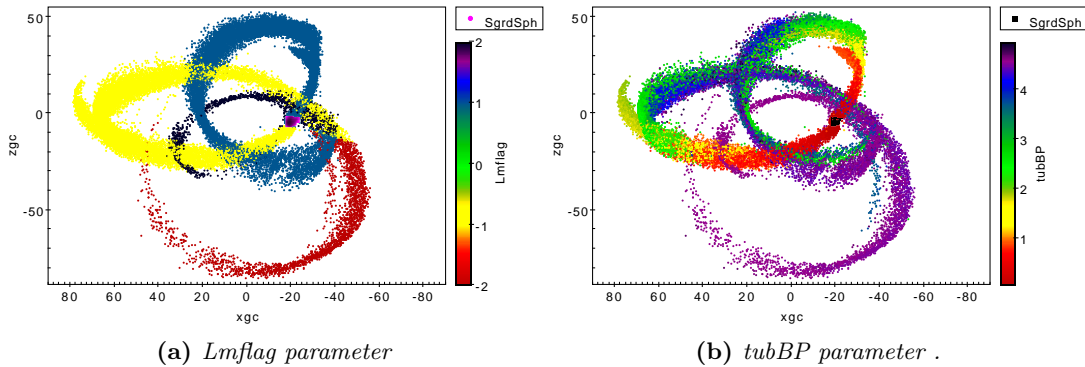


Figure 2.6 – Schematic plots created with the simulation files of Law & Majewski. **Panel a:** The *Lmflag* parameter specifies in which wrap a given particle is located. If $Lmflag = +1/+2$, it indicates the first/second wrap of the leading stream, while if $Lmflag = -1/-2$, it corresponds to the first/second wraps of the trailing stream. **Panel b:** the *tubBP* provides the time before present at which stars are unbound from Sgr main body.

2010 model¹. They simulate and predict the Sagittarius orbit. The graph shows both the leading and trailing streams that entirely wrap around the Galaxy. The colour-coding represents the time before present (*tubBP*) at which a particle became unbound from Sgr. The rough location of the massive GC is marked with a cross and lies at the centre of the main body of Sagittarius. It is now known that the leading arm exhibits a bifurcated density profile. In effect, there are two components: an old and fainter and a more recent and brighter stripe which are separated by $\sim 15^\circ$ on the sky (Belokurov et al., 2014). In 2012, Koposov et al. announced the existence of a bifurcated feature

¹ <https://faculty.virginia.edu/srm4n/Sgr/data.html>

also in the trailing arm crossing the Southern hemisphere where the bifurcation seems to follow almost a parallel track, as shown in fig.2.7. There is still much uncertainty regarding the formation of this bifurcated profiles. One hypothesis advanced takes into consideration the fact that two independent bodies (e.g. the original Sgr core and a companion dwarf) were bound when they fell into the MW potential (D’Onghia & Lake, 2008). In a recent paper (del Pino et al., 2020) it is speculated that a cause may be the inclination between the orbit and the internal angular momentum of Sgr. However, this system is so highly perturbed that an exact analysis of its dynamics is very complex to be attained and may require greater theoretical and computational endeavours.

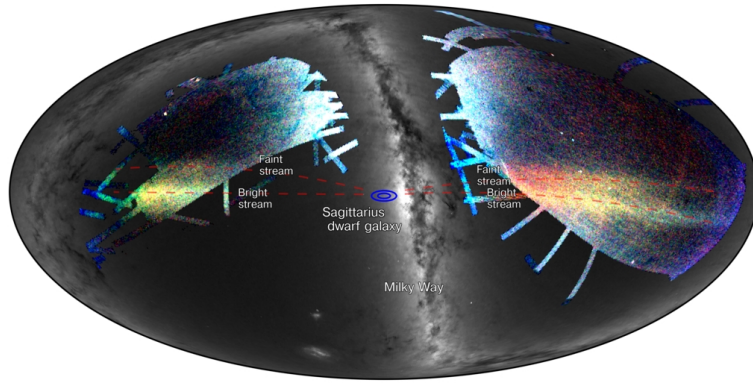


Figure 2.7 – *Sgr stellar streams. Fainter and brighter tails in the northern (right) and southern (left) hemispheres. Credit by Koposov et al.*

2.4 Orbit & Proper motion

As mentioned before, the Sagittarius merging is a unique event that proves an ongoing process of galactic merging and tidal disruption caused by its proximity and interaction with the Milky Way. The tidal stress induced on the dwarf system will eventually lead to the complete loss of its stars and globular clusters in favour of the Galactic halo. This “damage” inevitably marks its end which has been estimated to occur over the next Gyr (Vasiliev & Belokurov, 2020). Different investigations (Velázquez & White, 1995; Ibata, 1999; Vasiliev & Belokurov, 2020) have pointed out that the orbit of the dwarf satellite shows an elongation that is oriented along the tidal field created by our Galaxy (as it is illustrated in fig.2.8). This results in an alignment between the Sgr orbital plane and its direction of motion, which it is itself lined up with the Sgr stream (del Pino et al., 2020). Vasiliev & Belokurov (2020), thanks to the astrometric and photometric measurements from *Gaia* DR2, studied the 3D structure of Sgr and demonstrated that the vector describing its motion points parallel to its major axis, which in turn is aligned with the direction of the orbit. This finding confirms the fact that the prolate shape of Sgr, following the orbital direction, causes Sgr to be stretched across its major axis.

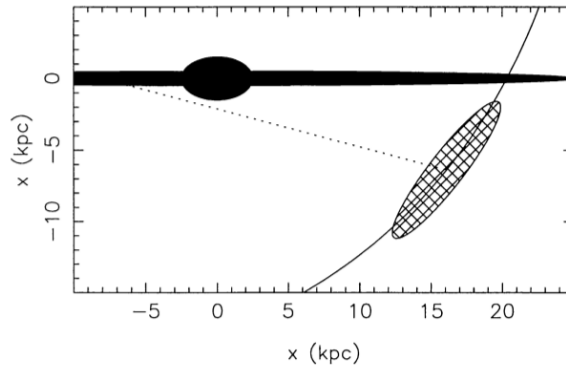


Figure 2.8 – *Simplified graph displaying the location of Sagittarius. The black dotted line shows the line of sight from the Sun to the dwarf satellite, while the solid line traces the orbital path of Sgr. The coordinates used denote the Galactic plane. It is visible that the orbital motion follows the major axis of the dwarf. Credit by Ibata, 1999.*

2.5 Stellar populations in Sagittarius

Not just the kinematics and dynamics of the dwarf galaxy are objects of study and investigation, but also many spectroscopic studies about the chemical properties of Sagittarius have been carried out during the years (e.g. Bellazzini et al. (1999); Carretta et al. (2010); Mucciarelli et al. (2017)). They all agree that Sgr is one among the most metal-rich and brightest dSph of the MW. The absolute magnitude is estimated to be $M_V = -13.27$ (Majewski et al., 2003). The existence of different stellar populations (SPS) has been unquestionably recognised in several investigations. This variety leads to a wide gradient in the values of metallicity and age. In fact, the metallicity and age spreads reported are respectively $-1.4 < [\text{Fe}/\text{H}] < 0.1$ and from 2 to 13 Gyr (Hasselquist et al., 2017).

Through the colour-magnitude diagrams for M54 and Sgr, Sarajedini & Layden (1995) identified a pronounced blue horizontal branch (BHB) belonging to the globular cluster and a red horizontal branch (RHB) as part of the Sgr galaxy. In the same study the authors confirmed the existence of RR Lyrae variables in M54 and derived $[\text{Fe}/\text{H}] = -1.79$ for the GC and $[\text{Fe}/\text{H}] = -0.52$ for Sgr dSph.

Later studies (Monaco et al., 2003) stressed again the existence of a span in metallicity within the dwarf galaxy. An intermediate age ($\sim 4 - 8$ Gyr) SP with $[\text{Fe}/\text{H}] \sim -0.2$ to -0.6 was recognised as the dominant population (more than 80%) in Sgr. An other important finding is the old metal-poor SP (age $\gtrsim 10$ Gyr; $[\text{Fe}/\text{H}] \lesssim -1.3$) that represents $\sim 10\%$ of Sgr galaxy (Monaco et al., 2003).

A considerable step forward in the studying of the stellar populations in the Sgr core has been made thanks to the Hubble Space Telescope (HST) Advanced Camera for Surveys (ACS). Thanks to the ACS data, detailed SP synthesis and analysis had been performed in the main body of Sgr (Siegel et al., 2007). This had led to the discovery of monotonically varying age-metallicity distribution, which, being caused by many star forming episodes, induced a chemical enrichment with time. Siegel et al.

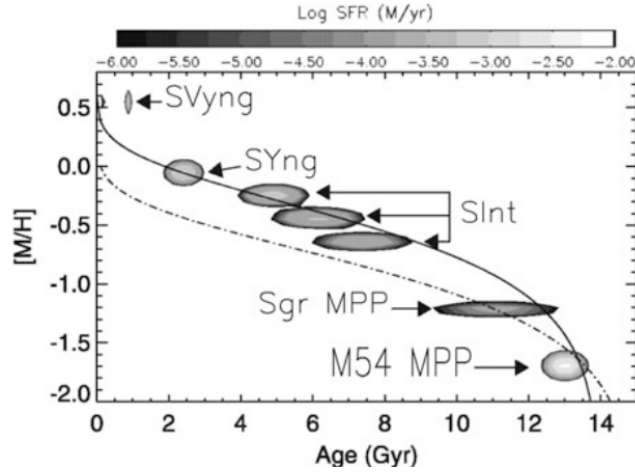


Figure 2.9 – AMR for Sgr core. From the ACS survey, (Siegel et al., 2007). M54 MPP: contribution from metal-poor M54 SP; Sgr MPP: metal-poor Sgr SP. SInt, SYng, SVyng represent respectively the intermediate-age, young and the very young populations.

revealed a very young SP of 0.7 Gyr with $[\text{Fe}/\text{H}] \sim +0.5$, a young one of 2.3 Gyr with $[\text{Fe}/\text{H}] \sim -0.1$, an intermediate SP aged 4.5 Gyr and a metal content of $[\text{Fe}/\text{H}] \sim -0.5$ and, finally an old and metal-poor SP of 13 Gyr with $[\text{Fe}/\text{H}] \sim -1.8$. The age-metallicity relation (AMR) for the Sgr core is depicted in fig.2.9.

The age and metallicity distributions of the dwarf galaxy reinforce the theory that Sgr,N and M54 are two distinct systems. In the paper of Bellazzini et al. (2008) the metallicity peak of Sgr,N is given around $[\text{Fe}/\text{H}] = -0.4$ and the distribution reaches solar metallicities. Additionally, Sgr,N is found to be dominated by an intermediate aged SP. On the other hand, the metallicity distribution of M54 shows its peak at $[\text{Fe}/\text{H}] \sim -1.45$ and its age is estimated to be ~ 13 Gyr. These results are additional proofs of the nature of Sgr as a nucleated dwarf galaxy.

Also the streams host different populations. A spread from $\langle [\text{Fe}/\text{H}] \rangle \sim -0.4$ (close to Sgr core) to $\langle [\text{Fe}/\text{H}] \rangle \sim -1.1$ (further away) had been measured by Bellazzini et al. (2006). This feature can be explained assuming that the original Sgr galaxy had a metallicity gradient, since the stars in the outskirts of the satellite galaxy are the first to become unbound (Tolstoy et al., 2009).

A recent paper about the Sgr streams (Johnson et al., 2020), deepening the study of the SPs in the stream, revealed that a diffuse metal-poor component is spread in space along the tails. The mean metallicity is indicated to be $[\text{Fe}/\text{H}] \simeq -0.99$ and its range $-3 \lesssim [\text{Fe}/\text{H}] \lesssim -0.2$. By emphasizing the importance of a metallicity dichotomy within the dwarf system, where the Sgr remnant is dominated by a more metal-rich component with $[\text{Fe}/\text{H}] \sim -0.4$, Johnson et al. suggest that there has been already a marked metallicity gradient in the original infalling Sgr dwarf galaxy. From these

outcomes, it is possible to speculate that the MP population was stripped away from the progenitor before the MR one. Within this perspective the MP sample presented in the streams has been even identified as the the “stellar halo” of the Sagittarius dSph galaxy.

2.6 Chemical composition

The several populations of the satellite are a clear clue that Sgr had a complicated star formation history (SFH) which does not extend until the present day, as its interaction with the MW left almost no gas behind. The idea of an extended SFH is supported by many studies about the chemical evolution of the system which show that Sgr has a deficit in $[\alpha/\text{Fe}]$, especially O and Mg (McWilliam et al., 2013). This composition proves that Sgr has been significantly enriched by delayed SN Ia products. The paucity of α elements along with $[\text{Na}/\text{Fe}]$, $[\text{Al}/\text{Fe}]$ and $[\text{Cu}/\text{Fe}]$ indicates a deficiency in the ejecta from SNII (McWilliam et al., 2013). One hypothesis to explain this scenario suggests a top-light or steep IMF for the system. This would mean that the recent generations of stars may have formed in an environment lacking massive molecular clouds that usually bring about the formation of more massive stars. A conflicting opinion is presented by Hansen et al. (2018), whose results about the chemical composition of Sgr (especially the results concerning the MP sample) suggested that more massive SNe ($\sim 13 - 15 M_{\odot}$) were progenitor stars in Sgr and thus enriched the later composition of the system before all the gas got lost or accreted the MW. Following this approach, Hansen et al., in strong contrast with McWilliam et al., discarded the idea of a top-light IMF. They found that short-lived and 15-25 M_{\odot} stars or even jets driven by SN are required to match and explain the composition attained with their chemical analysis of Sgr. The studies conducted by Hansen et al. used the delay model for SN Ia according to which the SNe are expected to explode 1-3 Gyr after the formation of the dwarf. They also found that Sgr lacks of light s-processed elements but on the other hand, the galaxy seems to be rich in heavy s-elements, like La and Nd (a clear difference from the MW which is abundant with r-process elements). This aspect may be referred to the presence of asymptotic giant branch (AGB) stars. Indeed, the AGB stars are believed to have a larger relative contribution to the chemical enrichment compared to the Milky Way, leading to a strong signatures of $[\text{La}/\text{Fe}]$, $[\text{Na}/\text{Fe}]$ and $[\text{Al}/\text{Fe}]$ (Hansen et al., 2018). The yield of neutron-capture elements elements is attributed to these metal-poor, low and intermediate-mass AGB stars which cause an enhancement in s-processed products. These stars are also hints for a leaky-box chemical evolution model. Such model predicts that the composition of the ISM is not completely homogeneous and the gas has been lost through star winds or supernovae explosions. Therefore, as time passes, the envelope ejections of lower and older stars may prevail in the gas composition. In this framework, the average value $[\text{Fe}/\text{H}] \sim -0.5$ of Sgr can be explained by the gas loss which weakens the for-

mation of higher metallicity stars (McWilliam et al., 2013). Additionally, the low and intermediate-mass AGB - in a binary configuration - are also in charge of providing the so-called Carbon Enhanced Metal-Poor stars (CEMP) that have been recently and for the first time detected in the dwarf galaxy (Sbordone et al., 2020). Even if Sgr dSph has been carefully studied during the last decade, large-scale surveys are still necessary to obtain a more precise and complete comprehension of this type of system and to gain detailed chemical analysis. These galaxies are faint objects and thus require large-aperture telescopes that could provide high-resolutions spectroscopic measurements.

Chapter 3

Data

In this thesis we study the metallicity distribution of Sagittarius. We are using Pristine Inner Galaxy Survey (PIGS) metallicity-sensitive photometry combined with spectroscopy from PIGS, APOGEE and CaT catalogues. We employ *Gaia* DR2 astrometry to select member stars. A summary of all steps is shown below. Where each point will be described in more details later in the chapter.

1. Cross correlation between the photometric catalogue provided by the Pristine Inner Galaxy (PIGS) Survey with *Gaia* DR2, available everywhere
2. Selection of the Sgr candidates using the *Gaia* DR2 astrometry; this step leads to the creation of a Sgr sample containing the pristine metallicity-sensitive photometry
3. Correction for the reddening effects by dust
4. Cross match between the Sgr footprint and the PIGS spectroscopic follow-up. This provides a catalogue for which spectroscopic $[\text{Fe}/\text{H}]$ and stellar parameters are available to test and guide our photometric analysis
5. Cross match between the PIGS photometric sample and the spectroscopic data provided by APOGEE DR16
6. Creation of the colour-magnitude (CMD) and colour-colour (CCD) diagrams showing the spectroscopic metallicities of PIGS follow-up and APOGEE
7. Application of the Calcium Triplet empirical formula on three spectroscopic data sets that provide the measurements of the Calcium equivalent widths which can be employed for inferring the metallicity values of the targets
8. Cross match between PIGS sample and the Calcium Triplet catalogues with the derived metallicity values
9. CMD and CCD displaying the derived CaT metallicities

| Catalogue | Type | Number of members |
|-------------------------------|---------------|-------------------|
| PIGS | Photometric | 23714 |
| PIGS follow-up | Spectroscopic | 418 |
| APOGEE | Spectroscopic | 744 |
| sgr_body_1 (From CaT dataset) | Spectroscopic | 2809 |
| sgr_body_2 (From CaT dataset) | Spectroscopic | 300 |
| sgr_body_3 (From CaT dataset) | Spectroscopic | 126 |

Table 3.1 – *List of the catalogues used for the data analysis. The type of catalogue is indicated for each sample together with the number of stars derived after being selected with the Gaia criteria to be members of Sgr.*

10. Comparison between the different catalogues

All these steps are required to then be able to perform an analysis on the metallicity distribution within Sgr dSph. The table 3.1 summarises all the catalogues used with the corresponding number of stars selected with the *Gaia* DR2 criteria for membership of Sagittarius.

3.1 PIGS Catalogue

As already stated in the Introduction 2.1, the Ca H&K photometry is extremely sensitive to the metallicity content of a star and therefore it facilitates the detection of MP stars around the MW and its satellites. To better study the behaviour of the MP stars present in the inner part of our Galaxy, a sub-survey of Pristine has been created: the Pristine Inner Galaxy Survey (PIGS, Arentsen et al. (2020)). Using the Pristine metallicity-sensitive photometric technique in combination with *Gaia* DR2 broadband *G*, *BP* and *RP* photometry (or alternatively PanSTARRs broad-band *griz* photometry), PIGS aims to seize a large sample of MP stars in the Galactic bulge. The PIGS coverage looks down to declination of -30° (see fig3.1) in the Northern hemisphere and it has been extended to low *b* to include also the Sgr region. We cross match the PIGS catalogue with the wide *Gaia* DR2 catalogue so to be able to isolate the Sgr members from the MW foreground and background stars using *Gaia* astrometry. The procedure followed is explained in the next section 3.2.

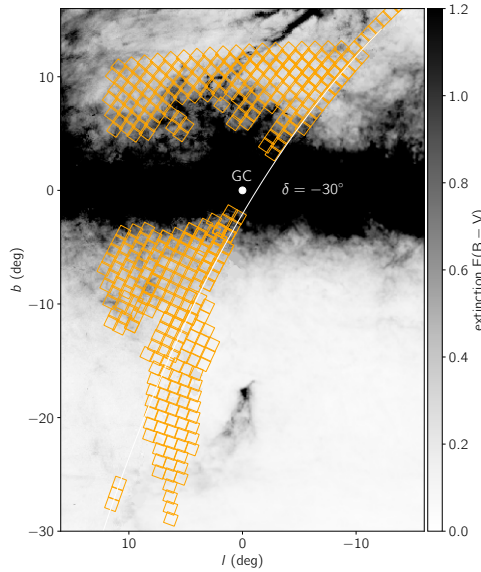


Figure 3.1 – *PIGS footprint*. The white line marks the region above a declination δ of 30° . Credit by Arentsen et al. (2020)

3.2 Sample selection

As already mentioned in the Introduction of Sgr (section 2.1) the location of the dwarf galaxy is not optimal as it lies on the opposite side of our Galaxy relative to the Sun and thus the contamination from the MW stars strongly affect the observations. Therefore, one of the first and fundamental steps in the analysis of Sgr is to isolate the Sgr member stars from the MW foreground and background stars. This part is performed using the astrometric measurements provided by the European Space Agency (ESA) mission *Gaia* (<https://www.cosmos.esa.int/web/gaia>)¹.

Gaia Data Release 2 (DR2) published on 25 April 2018 provides an homogeneous multi-band-all-sky photometry for ~ 1 billion targets brighter than 21 mag in G , together with a large radial-velocity survey for the brighter stars with $G=13$ (Gaia et al., 2018). Especially, the *Gaia* DR2 data set, with the extremely accurate proper motion (PM) measurements, enabled a careful and deep study about the dynamics of GCs and MW satellites. By providing precise high-precision parallax and proper motion measurements for the dwarf galaxies orbiting around the MW (Helmi et al., 2018), it has shed light on the existing interactions between our Galaxy and its satellites. The columns of the *Gaia* data that are used most extensively in this project are listed in Table 3.2.

As first step, we cross match the PIGS and *Gaia* samples. To better confine the dwarf system we avoid the area corresponding to the MW bulge region eliminating stars with $|l|$ and $|b| \lesssim 10^\circ$. The desired region is represented in the figure 3.2, where

¹processed by the *Gaia* Data Processing and Analysis Consortium (DPAC, <https://www.cosmos.esa.int/web/gaia/dpac/consortium>). Funding for the DPAC has been provided by national institutions, in particular the institutions participating in the *Gaia* Multilateral Agreement.

| | | |
|---|---|------------|
| Source_id | Gaia unique label for each star | |
| RA (α) | Barycentric right ascension in ICRS | [deg] |
| DEC (δ) | Barycentric declination in ICRS | [deg] |
| π | Absolute stellar parallax | [mas] |
| l | Galactic longitude | [deg] |
| b | Galactic latitude | [deg] |
| PM ($\mu_\alpha^* = \mu_\alpha * \cos(\delta)$) | Proper motion in right ascension in ICRIS | [mas/year] |
| PM (μ_δ) | Proper motion in declination in ICRIS | [mas/year] |
| PHOT_G_MEAN_MAG | G band mean magnitude | [mag] |
| PHOT_BP_MEAN_MAG | Integrated BP mean magnitude | [mag] |
| PHOT_RP_MEAN_MAG | Integrated RP mean magnitude | [mag] |
| D | Astrometric excess noise | |
| BP/RP excess flux | excess of flux in <i>BP</i> and <i>RP</i> | |
| ruwe | Renormalised unit weight error | |

Table 3.2 – List of the used Gaia DR2 parameters

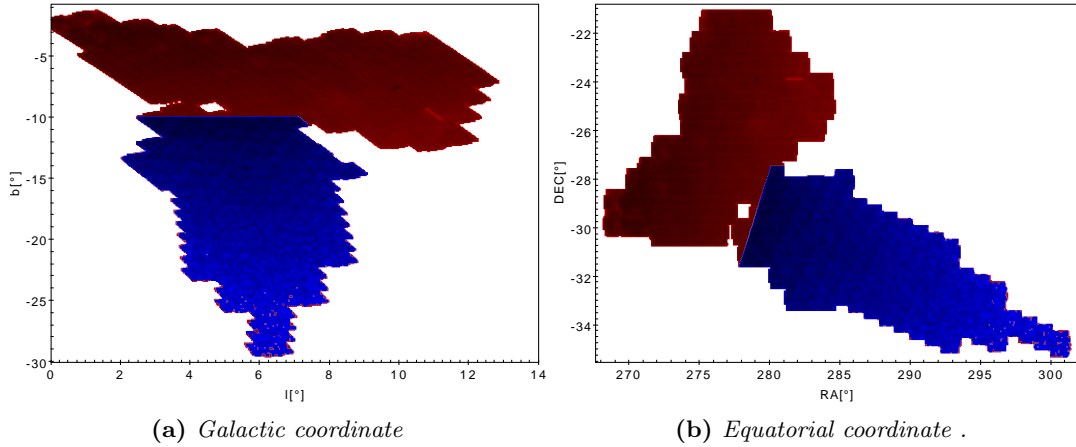


Figure 3.2 – **Panel a:** Selection of the Sgr stars in galactic coordinate: the blue part represents the dwarf galaxy while the red area identifies the entire PIGS footprint which is still contaminated by the MW stars. **Panel b:** Same selection in equatorial coordinate of right ascension (RA) and declination (DEC).

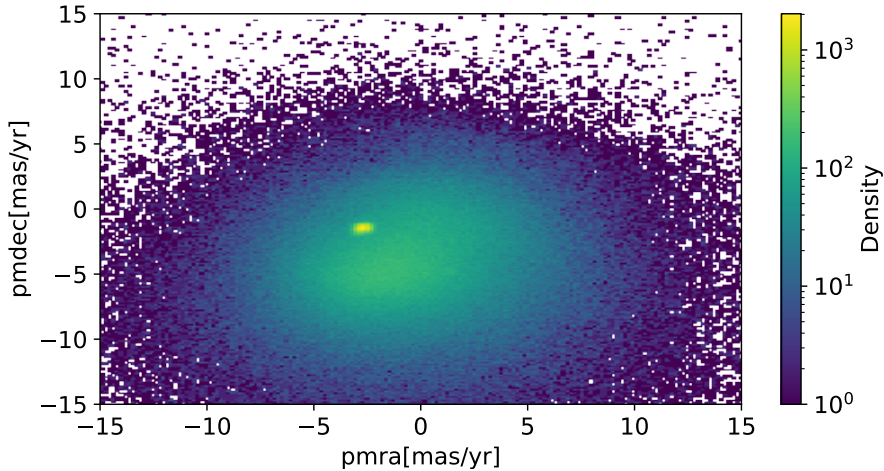


Figure 3.3 – Zoom in the PM space of the photometric catalogue of Gaia DR2. The plot is already the outcome of a cut in parallax for getting rid of the MW populations. By fixing a radius of 6° around the position of the GC M54 we arrive to define the yellow overdensity, representing Sgr dSph that stands out against the MW stars.

it appears respectively in galactic and equatorial coordinates. The red parts represent the overall PIGS coverage, while the blue region will be used for the study of Sgr. Secondly, in order to eliminate the contamination from the foreground MW stars that stand within 20 kpc between us and Sgr, we decide to perform a cut in parallax of $\pi - \sigma_\pi < 0.05$. This cut may seem quite “aggressive”, but it is reasonable since it is combined to a wider cut in proper motion. Indeed, we use a circle of radius 0.6 mas/yr centred around $\text{pmra} \sim -2.69$ mas/yr and $\text{pmdec} \sim -1.4$ mas/yr to be able to limit the member stars of Sgr. In plot 3.3 it is possible to appreciate Sgr sticking out from the MW foreground stars as a clear yellow overdensity in PM space. This wider cutoff in PM space is justifiable as the centre of the proper motion changes along the body of Sgr (Vasiliev & Belokurov, 2020). After trying different cut combinations, we reach the conclusion that making a cut with stricter parallax but wider proper motions enables to have more Sgr candidates than the reverse way and it creates a sample with more stars providing thus a better statistics.

However, the choice of fixing the same average PM values along the entire Sgr body is not entirely justifiable, as Sgr does not show a constant proper motion but the value changes within the galaxy due to a projection effect (Vasiliev & Belokurov, 2020). This variation is not necessarily correlated with internal motions in Sgr, such as its streams and disruption, but it is caused mainly by a perspective distortion. Therefore, it is possible that the Sgr selection performed with the PM values breaks moving along the main body. This effect, playing a major role in the study of the metallicity distribution, will be analysed and corrected in the data analysis part.

To further test the Sgr selection we decide to apply some additional quality filters on *Gaia* astrometry and photometry that appeared in a paper recently published by Vasiliev & Belokurov (2020). In their work the authors also employ *Gaia* DR2

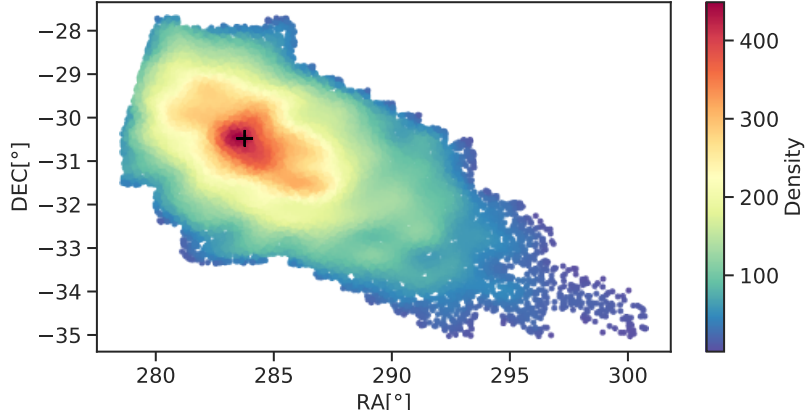


Figure 3.4 – The data points are from the *Gaia* DR2 photometric catalogue cross matched with the PIGS data sample. The plot represents the density of the stars selected as member of Sagittarius galaxy. The cross indicates the position of the GC M54.

data for the membership selection of Sgr stars. In addition to the cuts in magnitude ($13 < G < 18$) and parallax ($|\pi| \leq 5 \times \sigma_\pi$) they use three other constrains: `astrometric_excess_noise` < 1 , `RUWE` < 1.3 and `phot_bp_rp_excess_factor` $< 1.3 + 0.06 \text{phot_bp}^2$. The first filter avoids that the residuals between an observation of a source and its fit are statistically large. The `RUWE` parameter is associated with the Renormalised Unit Weight Error of each *Gaia* source. A value > 1.4 may be an indication that the source does not provide a good fit to the astrometric observation (Lindgren et al., 2018). Lastly, the condition on the BP/RP excess flux checks for an inconsistency between the G_{BP} and G_{RP} passbands. Making use of these filters we are sure to eliminate from our sample “bad” *Gaia* photometric and astrometric data.

The final Sgr selection accounts for 23714 members which are displayed in the footprint in fig.3.4 colour-coded by the stellar density. Because of the cross-matched sample that we started with, we have Pristine photometry available for each of these stars - and thereby the potential to investigate their metallicities. As can be seen from the graph, the number of stars is rather higher at the centre (where the GC M54 is indicated with a black cross), and it drops markedly moving towards the edge of the body.

To test once again the Sgr member selection it would be also possible to use the radial velocity measurements. However, being this information only available for the spectroscopic samples, we choose not to constrain the Sgr selection using the RV data as it would be a cut that just concerns a part of the catalogues. On the other hand, it is interesting to see if the spread of the RV values is in agreement with the member selection performed. In this regard we plot a normalised histogram containing the RV data for all the spectroscopic samples described below (created after the membership selection) which is shown in fig 3.5. From the graph is possible to see that there are almost no outliers from the main distribution. Therefore it gives us confidence that our candidate selection works properly.

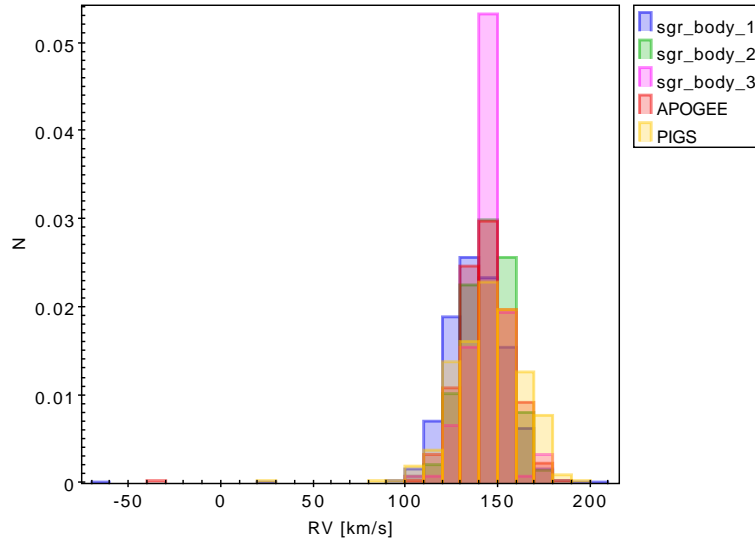


Figure 3.5 – Normalised histogram for the radial velocities of the spectroscopic catalogues constrained to contain only Sgr stars. The samples named “sgr_body_1, sgr_body_2, sgr_body_3” belong to the CaT dataset. The APOGEE and PIGS follow-up samples are coloured respectively in red and yellow. The catalogue which appears with the name “sgr_body_3” corresponds to the one that includes the M54 region. It is narrower respect to the other distributions since it covers a very small region of the galaxy.

3.3 Extinction correction

The position of the dwarf galaxy, apart from making observations difficult due to the high number of MW stars, is aggravated by the presence of dust that introduces inevitably a reddening effect which influences the photometry. We create an extinction map for the region of Sgr which is shown in fig 3.6. We can observe the excess colour being higher moving in the direction of the galactic centre and around M54, where the amount of reddening (characterised by the colour excess $E(B - V)$) is estimated in B and V bands to be ~ 0.15 . The object’s colour excess used comes from Schlegel et al. (1998) who created a full-sky map of Galactic dust reddening known as “SFD”. This quantity represents the dust absorption. For eliminating this effect from the magnitudes of the Sgr stars, we use the formula $m_0 = m - A_m \times E(B - V)$ (where m_0 indicates the magnitude corrected for extinction) for the bands G , BP and RP . We employ the following extinction coefficients: $A_G = 2.563$, $A_{BP} = 3.332$ and $A_{RP} = 2.219$ (Arentsen et al., 2020).

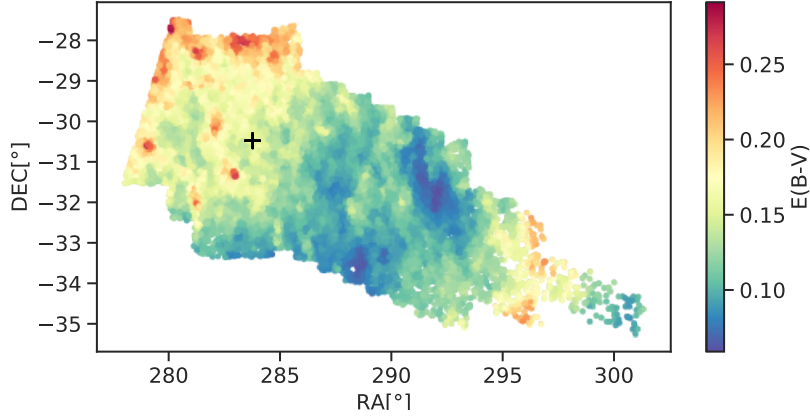


Figure 3.6 – The figure shows the coverage of the PIGS Sagittarius footprint with colour-coded the extinction map for Sgr dSph. The colour-bar values, given by Schlegel et al. (1998) extinction map, suggest that the reddening increases moving towards the galactic centre (RA $\approx 266^\circ$ & DEC $\approx -28.9^\circ$). The cross symbol traces the position of the GC M54

3.4 Description and analysis of the available spectroscopic samples

In this section we introduce and comment the metallicity analysis obtained thanks to three spectroscopic data samples: the PIGS spectroscopic dataset, the APOGEE dataset and a collection of stars that we have access to with spectroscopy in the CaT wavelength region (8498-8662 Å). While APOGEE and the PIGS follow-up offer direct measurements of the iron content of their targets, the CaT dataset provides the measurements of the Calcium triplet equivalent widths. It is therefore necessary to go through a specific relation (3.1) to obtain the corresponding $[\text{Fe}/\text{H}]$ values. Before proceeding with the discussion about the metallicity distribution, we compare the results of the CaT technique with the spectroscopic metallicities provided by APOGEE.

3.4.1 PIGS follow-up

A 3-years long PIGS follow-up has been carried on with the aim of identifying in the inner galaxy VMP stars via the Ca H&K photometry. This catalogue contains ~ 13000 objects of which about 8000 have already been presented in Arentsen et al. (2020) and for each star it provides the spectroscopic $[\text{Fe}/\text{H}]$ values derived through full-spectrum fitting of low/intermediate resolution spectra using the FERRE code. (Prieto et al., 2006). In addition to this catalogues a recent set of data had been observed in June 2020. It has been later analysed and inserted in the follow-up. To use its spectroscopic information we start performing a cross-correlation between PIGS photometry and its spectroscopic follow-up. Their overlap is visible in fig 3.7. The obvious irregular

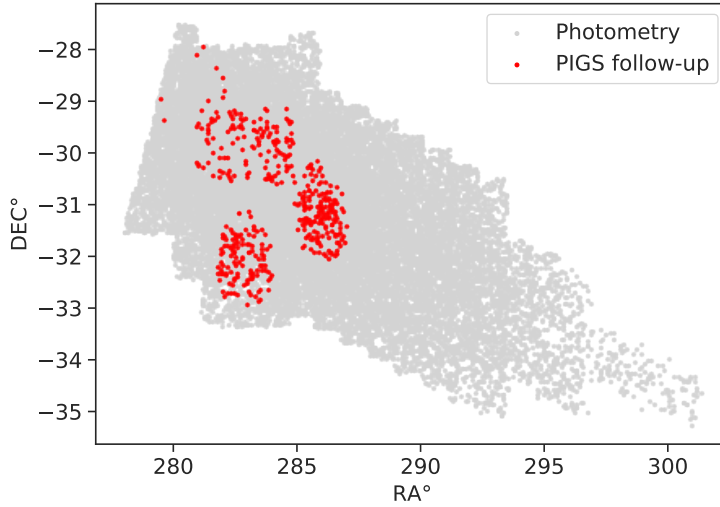


Figure 3.7 – The targets from the PIGS follow-up (observed until June 2020) are superimposed in red on the Sgr footprint (colored in gray). The inhomogeneous spread may cause some asymmetries in the metallicity distribution analysis for Sgr.

distribution of the spectroscopic data over the body is likely to affect statistically part of the analysis and thus it is important to consider this aspect in the interpretation of the final results. Moreover, this catalogue aims to detect very metal-poor candidates, and therefore its bias towards the selection of lower metallicities is considerably strong and will be evident in the study of the metallicity for the Sgr dSph.

3.4.2 APOGEE catalogue

The Apache Point Observatory Galactic Evolution Experiment (APOGEE) is a large infra-red spectroscopic survey which has a public data release. It includes spectra, stellar parameters, and elemental abundances for $\sim 100,000$ stars from different regions of the MW. APOGEE uses a high-resolution spectrograph ($R \sim 22500$) operating in the H-band that takes the spectra for more than 100,000 stars across the MW among which thousands of red giants. In the 16th data release part of the observations selected some Sgr member stars and attempted to isolate the red giant branch present in the core of the dwarf. By providing many different chemical abundances, the release draw a complete picture of the chemical pattern of the galaxy (Hasselquist et al., 2017). The catalogue used in the thesis is *AllStarLite*. It contains the latest infra-red spectra of the SDSS (Sloan Digital Sky Survey) component Apache Point Observatory Galaxy Evolution Experiment 2 (available at https://www.sdss.org/dr16/irspec/spectro_data/) and it is the fourth phase of the SDSS. We cross match the Sgr footprint containing the Pristine photometry with the APOGEE sample. The number of selected objects is 744 and the resulting overlap is displayed in fig. 3.8.

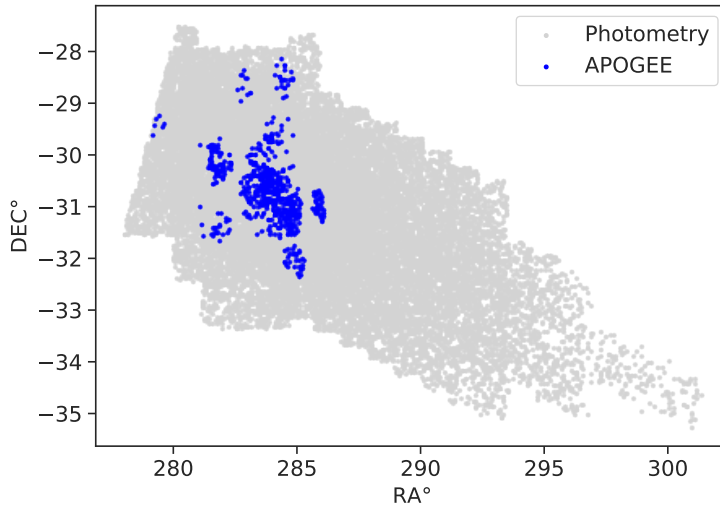


Figure 3.8 – *Overlap between the photometric (in grey) and spectroscopic data from APOGEE (blue) selected to cover the Sgr footprint.*

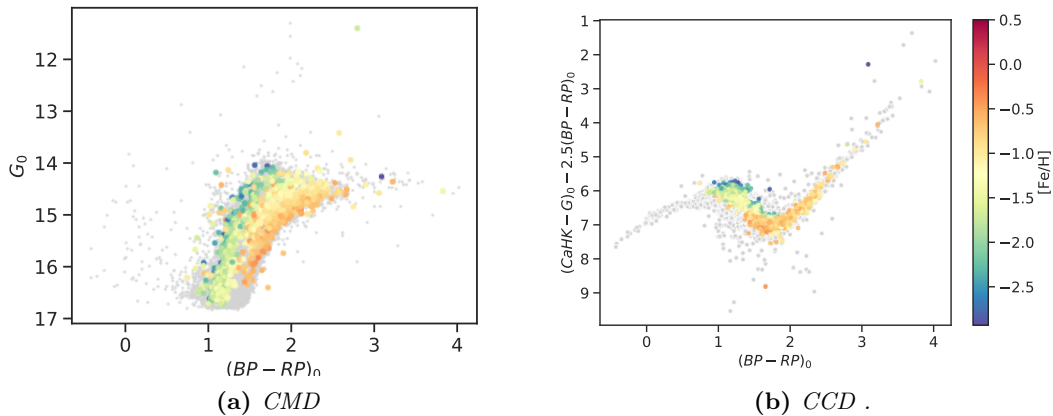


Figure 3.9 – *CMD & CCD for the Sgr footprint. **Panel a:** The $[Fe/H]$ values contains both PIGS and APOGEE metallicities **Panel b:** Colour-colour diagram showing the same metallicity scale of the CMD. In the y-axis appears the terms referring to the Pristine photometry that allows a clear spread in metallicity that ranges along the vertical axis.*

PIGS & APOGEE metallicities

The PIGS follow-up and the APOGEE spectroscopic catalogues, providing direct $[Fe/H]$ measurements, offer the possibility to straightly display their colour-magnitude (CMD) and colour-colour (CCD) diagrams. We merge the metallicities of the two samples in the graphs reported in the panel 3.9. It is interesting to notice that in the y-axis of the CCD (as well in all the CCDs that follow and which will be presented in this work) appears the Pristine Ca H&K photometric term. This term is used to

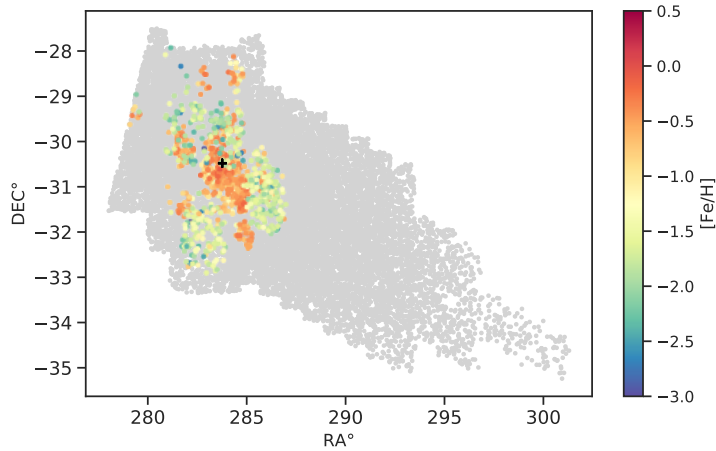


Figure 3.10 – *Sgr* footprint colour-coded in function of the $[Fe/H]$ values provided by APOGEE and the PIGS spectroscopic follow-up. The bluer constituents are given by PIGS while the higher $[Fe/H]$ targets are part of the APOGEE sample.

create a colour space which allows a clear spread in the $[Fe/H]$ values along the vertical axis and that will enable us in a later stage of the project to perform a metallicity cut to distinguish the MP from the MR population. It is promptly noticeable that the metallicity budget from these two catalogues is rather metal-poor, especially if we compare it with the one that will be derived for the CaT catalogues (sect. 3.4.3). This is due to the fact that the PIGS survey, being biased towards the research of metal-poor stars, contributes with many lower metallicity stars.

Indeed, observing fig 3.10, the stellar contribution from PIGS is the one represented in bluish colours and it denotes a lower $[Fe/H]$ content. On the other hand, the APOGEE survey has not specifically selected lower metallicities, therefore its metallicity is closer to the one provided by the CaT dataset with a more metal-rich metallicity budget.

3.4.3 The CaT catalogues

Another important contribution of the spectroscopy used in this project is given by the CaT dataset. It is constituted of four catalogues provided by R. Ibata, private communication. Some of the data already appeared in previous studies about the Sgr dSph and M54 (Bellazzini et al., 2008). These three catalogues cover the Sgr main body and they are illustrated in the plot 3.11 in three different colours. The fourth comprises the Sgr stellar tails. The catalogue denominated as “sgr_body_1” and the one that covers the Sgr streams (which does not appear here) are observed with the AAT telescope using 2dF+AAOmega. The catalogues called “sgr_body_2” and “sgr_body_3” are taken with VLT using FLAMES.

On these catalogues we apply the same cuts and cross-matches indicated in sect. 3.2 to define the Sgr membership. The resulting candidates are 2809, 300 and 165 for

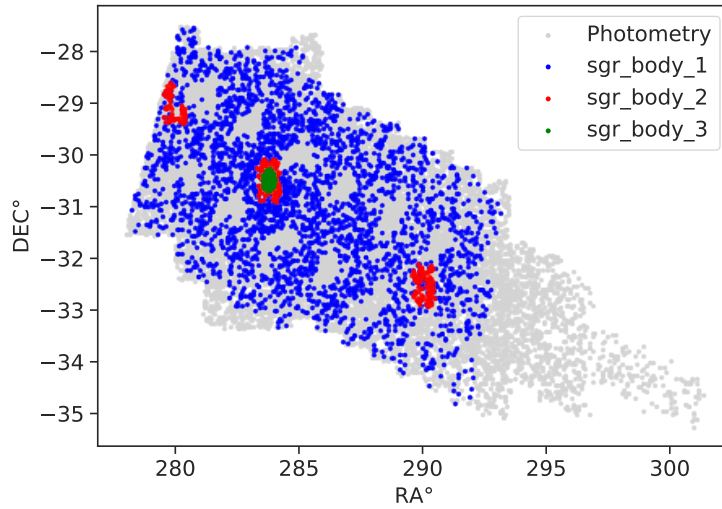


Figure 3.11 – Spatial coverage of the three CaT catalogues overlapped with the PIGS photometric sample. The unusual pattern shown by “sgr_body_1” is possibly due to the instrument used during the observations. It is likely that it has a circular field of view that produces these visible different pointings on the footprint.

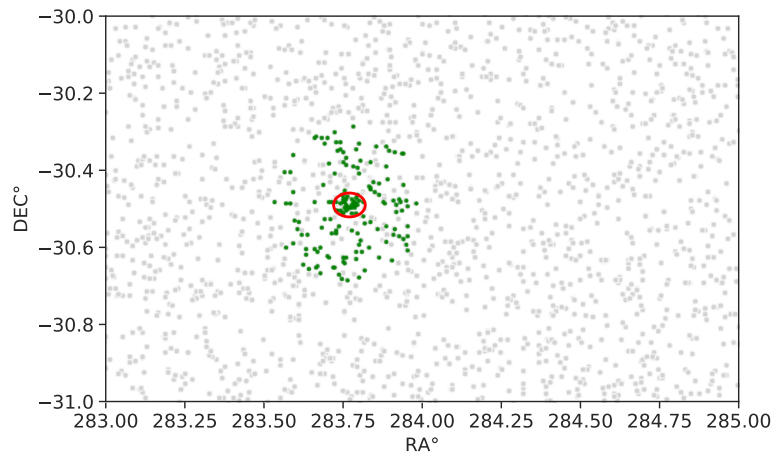


Figure 3.12 – Equatorial coordinates zoomed in on the very central region where M54 lies. The red ellipse delimitates the stellar density that we removed to eliminate the stars which are likely part of the GC.

sgr_body_1, sgr_body_2 and sgr_body_3 respectively. Concerning this last sample, we realized at the moment of studying the metallicities of Sgr that a further constrain was required. This latter is necessary to avoid the inclusion of too many stars belonging to the GC M54. In fact, looking later at the colour-magnitude and colour-colour diagrams of this catalogue, we become conscious of the contamination caused by the stars of M54. Moreover the Pristine photometry is not particularly effective in very crowded regions, as the one where M54 dominates. We thus decide to eliminate the stellar overdensity

that lays at the very centre of Sgr which corresponds to the spatial region of M54 (fig 3.12), reducing the number of stars to 126. The exclusion of the M54 stars is also reported in the *Gaia* paper about the kinematic of GCs and dwarf galaxies around the MW (Helmi et al., 2018). After having removed the star sample identified as M54 in the spectroscopic catalogue, we decide to exclude this same region in all of the photometry to avoid areas which are not suitable for the Pristine metallicity-sensitive photometry.

The Calcium Triplet method

The CaII triplet (CaT) technique is an empirically developed and calibrated method which has been devised by Armandroff & Da Costa in 1991. Its aim was to calculate the [Fe/H] for Red Giant Branch (RGB) stars relying on the strength of the CaT lines at $\lambda = 8498, 8542, 8662 \text{ \AA}$ (see fig.3.13). The strength of these absorption lines depends directly on the line opacity divided by opacity of the continuum. An indication of this physical quantity is provided by the equivalent widths (EWs) of the lines. These lines are found in the NIR region, a favourable position as the red giants emit more flux in this area. In this part the continuum of the spectrum is relatively flat (because there are not a lot of other features) and thus advantageous for the definition of the CaT widths.

Armandroff & Da Costa found out that the dependence of the lines on different parameters weakens ascending the red giant branch (RGB). Therefore, by including the position of the stars in the RGB (with respect to the horizontal branch) the effects of T_{eff} and $\log(g)$ can be eliminated. Following this approach, they defined instead of the EW a new parameter called the “reduced equivalent widths” (W') of λ_{8542} , λ_{8622} , that correspond to the second and third lines of the triplet EW_2 and EW_3 . The W' indicates the line strength at the level of the horizontal branch (HB). This parameter incorporates the RGB stars above the branch and it includes a term referring to the mean magnitude of the HB (V_{HB}), which is needed to remove the dependence on reddening and distance. The first line λ_{84982} of the triplet can be neglected because it is the weaker of the triplet and thus adds noise in the determination of the CaT. With this definition, it was empirically demonstrated a direct correlation between W' and [Fe/H] (Armandroff & Da Costa, 1991). This relationship established that the strength of the CaT lines increases with the metallicity. This link makes therefore the calcium triplet lines a powerful tool to discriminate the metallicity of a star.

Usually, this empirical formula was calibrated on GC stars, as they form part of a single SP and thus have the same age and metallicity (at least the Ca and Fe elements). However, for investigating the metallicity of more complex systems, such as dwarf galaxies, many studies have been dedicated to the application of the CaT method in the case of several SPs that inevitably lead to a gradient in metallicity and age. In this framework, the CaT method can be further employed in the research of EMP stars in nearby and distant dwarf galaxies. Indeed, it had been shown (Starkenburger et al., 2010) that applying the CaT method on the RGB stars of dwarf galaxies is

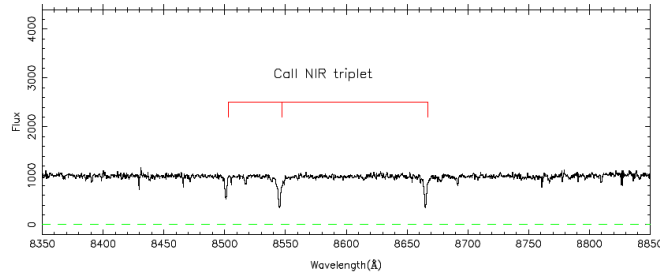


Figure 3.13 – An example of a LR spectrum. The Calcium triplet lines are marked with the red line. Credit by Battaglia et al., 2008

possible and it aids constraining their chemical evolution processes and history. In fact the Ca lines, even down to metallicities of < -3 (Starkenburg et al., 2010), are good indicators of the primordial chemical composition of a star as they are not strongly affected -as other elements- by nucleosynthesis processes (Armandroff & Zinn, 1988). In 2008, Battaglia et al. presented an empirical relation between $[\text{Fe}/\text{H}]$ and the equivalent widths of the Calcium lines for inferring the metallicity range $-2.5 < [\text{Fe}/\text{H}] < -0.5$ of RGB stars in dSphs. They noticed that for lower metallicities the CaT method is robust despite the existence of a gradient in age, $[\text{Fe}/\text{H}]$ or $[\alpha/\text{Fe}]$ elements. For estimating the EWs, Battaglia et al. used a Gaussian profile for fitting each CaT spectral line. By comparing over a wide range of metallicity values the CaT equivalent widths with the values of $[\text{Fe}/\text{H}]$ (obtained via high resolution spectroscopy), it has been possible to establish a relation between the EWs of CaT and $[\text{Fe}/\text{H}]$. The real line is a function of many different parameters (e.g. $[\text{Fe}/\text{H}]$, $\log(g)$, T_{eff}) and its wings, laying on the part of the curve growth where the core of the line saturates, do not show a perfect Gaussian shape, but they are rather damped as the EW increases. This behaviour can be explained by the fact that the lines are so strong that they saturate in their cores. To correct this effect Battaglia determined the best fit slope between the Gaussian fit and the direct integration of the lines. The value of the slope, which is estimated to be around 1.1 (see fig.3.14) will be used during the data analysis (chapter 4).

Later studies, by performing spectral analysis on the Ca II triplet (Starkenburg et al., 2010), discovered that the linear relation proposed by Battaglia et al. breaks down starting from $[\text{Fe}/\text{H}] < -2.0$. Indeed, at low $[\text{Fe}/\text{H}]$ values the EW of the line is considerably less sensitive to variation in gravity or temperature of the stars and the metallicity calculated with the linear empirical relation is highly overestimated. It was also noticed that the broadening of the CaT wings decreases along with the metallicity, as the EW is dominated at higher $[\text{Fe}/\text{H}]$ by the wings of the line as can be seen in fig. 3.15. The change of the line shape is also due to the presence of some nearby absorption lines that are likely to be included in the Gaussian fit of the line. The hydrogen Paschen lines are a remarkable example of this occurrence. It is indeed possible that, for hotter stars, they become embodied in the wings of the Triplet and

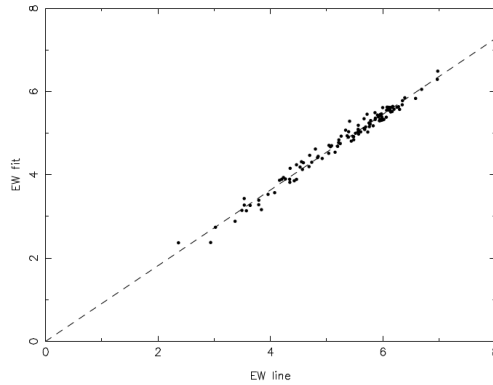


Figure 3.14 – Relation between the EW fit (*EW fit*) and the direct integration of the lines (*EW lines*). By inferring the slope of the correlation it is possible to take into account the non perfect Gaussian shape of the CaT lines. Credit by Battaglia et al., 2008

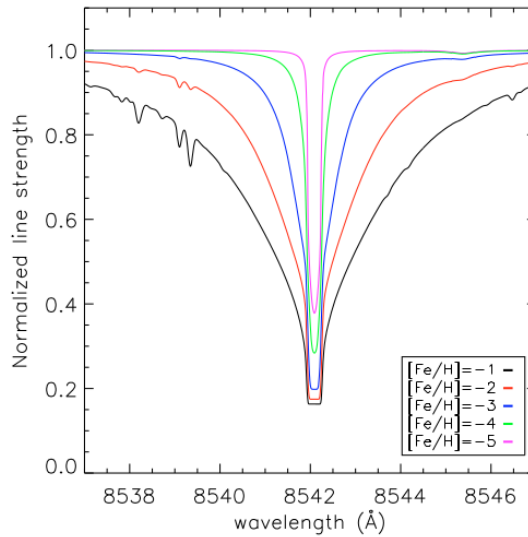


Figure 3.15 – Here it is displayed the variation of the CaT line for different metallicity values. The flattening of the core is appreciable for higher $[Fe/H]$ values, while for lower metallicities the wings dominate the line shapes. Credit by Starkenburg et al., 2010

thus affect the measurements of their EWs. Another concern taken into consideration by Starkenburg et al. is the study of the effects induced by the α elements on the CaT lines. Since the strength of the lines is affected by the presence of free electrons, the $[\alpha/Fe]$ quantity has to be considered in the conversion of the EWs to metallicity. Nevertheless, in the range of metallicity and $(V - V_{HB})$ stated above it has been shown (Starkenburg et al., 2010) that the $[Fe/H]$ value influences the EW more than the α elements. Taking into account all of these effects, Starkenburg et al. presented a new calibration (formula 3.1) that covers a metallicity regime down to $[Fe/H] \geq -4$:

$$\begin{aligned}
 [\text{Fe}/\text{H}] = & -2.87 + 0.195 \times (V - V_{HB}) + 0.458 \times EW_{2+3} \\
 & -0.913 \times EW_{2+3}^{-1.5} + 0.0155 \times EW_{2+3} \times (V - V_{HB})
 \end{aligned} \tag{3.1}$$

This formula aims to fit the predominant features that appear at low-metallicity values so to be able to trace the EMP stars around the MW and its satellites. It is calibrated over a metallicity range that has as upper limit $[\text{Fe}/\text{H}] = -0.5$, as for higher values the CaT lines are so dominated by their wings that this relation does not hold any more and the flux of the line is saturated due to the absorption. Following the idea of Armandroff & Zinn the formula operates only on RGB stars above the HB, it is therefore valid only over the range $-3 < V - V_{HB} < 0$ in order to avoid fainter stars on which the relation is less effective. In conclusion, this technique is a solid and powerful tool to look for MP stars requiring only the absolute magnitude of the target and a small spectral region of its spectrum.

Application of the CaT relation

Since the three CaT catalogues do not present the metallicity values for the observed stars, it is required to apply the formula 3.1 that connects the EWs measurements to the $[\text{Fe}/\text{H}]$ values. The procedure followed is summarised in the next points:

1. Because the CaT empirical relation is not properly constrain on stars closer to the HB (Starkenburg et al., 2010) we apply the cut $-3 < V - V_{HB} < 0$ to exclude those stars below the HB that deviate strongly from the CaT relation
2. We sum the EW of the second and third line multiplying by a correction factor of 1.1 (for the reason discussed in section 3.4.3). We take the absolute value of the sum because the EW values (which indicate the areas covered under the continuum) are presented in the CaT dataset as “negative” values, while in the CaT relation they are defined by Starkenburg et al. as “positive” values ²:

$$EW_{(2+3)G} = 1.1 \times |EW_2 + EW_3|$$

3. We correct the magnitudes for the extinction effect:

$$G_0 = G - E(B - V)_{\text{sfd}} \times 2.563$$

$$(BP - RP)_0 = BP - RP - E(B - V)_{\text{sfd}} \times (3.332 - 2.219)$$

4. We transform them into the V band using the *Johnson-Cousins* relationship (Evans et al., 2018):

$$(G - V)_0 = f_1 + f_2 \times (BP - RP)_0 + f_3 \times (BP - RP)_0^2$$

The coefficients are provided in the *Gaia* paper about the photometric content of the second release (Evans et al., 2018) ³

² $EW_{(2+3)G}$, the G letter stands for Gaussian, since this term is multiplied by the factor 1.1 to correct the non perfect Gaussian wings of the absorption line

³ $f_1 = -0.01760$, $f_2 = -0.006860$ and $f_3 = -0.1732$

5. The value of the mean magnitude in the V band is set to: $V_{HB} = 18.16$ (Harris, 2010) and corrected for reddening: $V_{(HB)_0} = 18.16 - 2.742 \times 0.15$, where $E(B-V) = 0.15$ and the V band extinction coefficient are provided by Schlegel et al. (1998)
6. Finally, having all the terms required by the CaT relation, we can infer the $[Fe/H]$ values for the CaT dataset

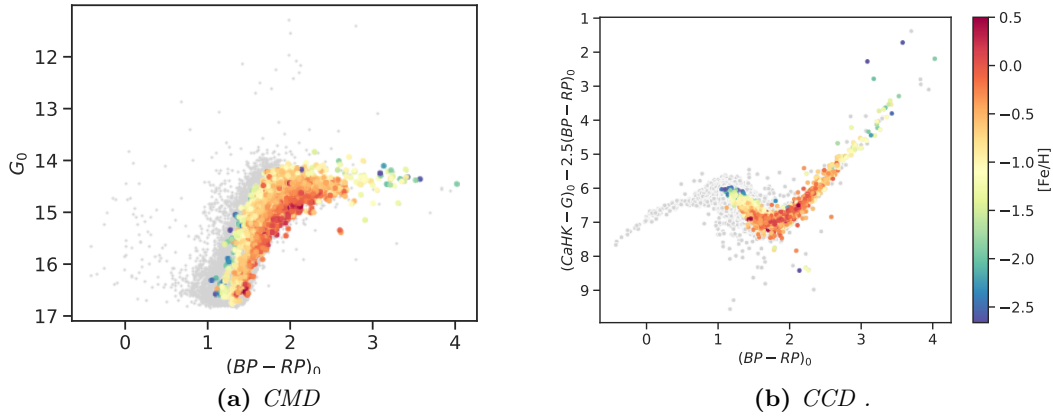


Figure 3.16 – *CMD & CCD for the Sgr footprint. Panel a:* The colour-magnitude diagram in $BP-RP$ and G magnitudes for the Sgr selection. The grey dots represent the photometric sample for the Sgr system and the colour-coding reports the metallicity values calculated with the CaT relation. **Panel b:** Colour-colour diagram showing the same metallicity colour-coding used for the CMD.

Once the $[Fe/H]$ values have been derived for all the targets, we are able to create the CMD and CCD with the metallicity results computed via the calibration formula, fig. 3.16. It is important to keep in mind that for $[Fe/H] > -0.5$ the CaT relation shows systematics and the formula can not be applied with complete confidence (Battaglia et al., 2008). The plot 3.17 shows the spatial distribution of the stars belonging to the CaT dataset colour-coded by the calculated $[Fe/H]$ values. Looking at the figure, it is noticeable that these catalogues contains on average mostly MR stars. This can be partially due to the fact the CaT catalogues are pre-dating *Gaia* astrometry, therefore it is probable that more MR stars have been selected as they stick out more clearly in the CMD that had been used to separate the Sgr members from the Milky Way bulge stars.

3.5 Catalogues comparison

Before proceeding with the study of the metallicity distribution of Sgr, we compare the results of the CaT technique with the other spectroscopy. We use the APOGEE catalogue for the comparison as it has the largest overlap and we compare it with

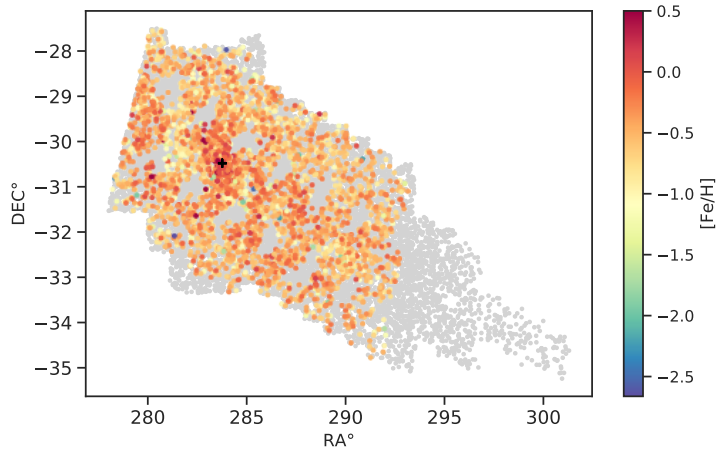


Figure 3.17 – *Sgr* footprint colour-coded in function of the $[Fe/H]$ values calculated with the *CaT* formula. The average metallicity indicates a dominant MR component for the *CaT* dataset.

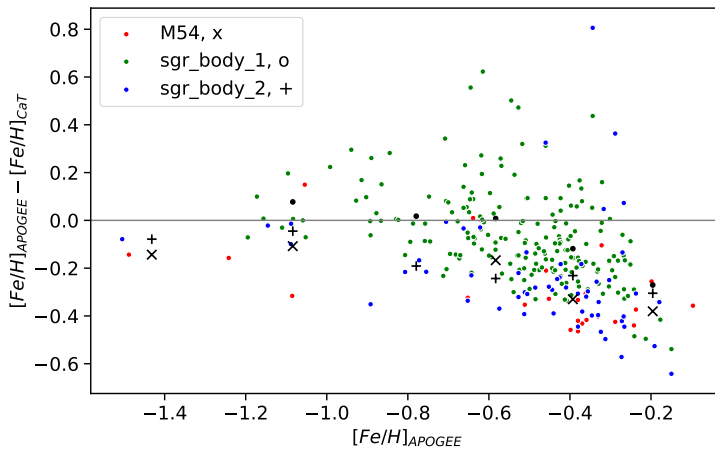


Figure 3.18 – The *x*-axis displays the spectroscopic $[Fe/H]$ values from APOGEE while the vertical axis shows the difference between APOGEE and the *CaT* metallicities. The different *CaT* catalogues are differentiated by three colours. The black symbols identify the average difference in metallicity bins of 0.3 dex. Moving towards higher metallicities the dispersion increases, meaning that the results given by the *CaT* formula deviate more from the spectroscopic values.

the three *CaT* catalogues each displayed in a different colour in the graph 3.18. This confirms that the *CaT* relation gets worse at the high $[Fe/H]$ end. In fact, at higher metallicities, the *CaT* results deviate more from the spectroscopic values than at lower metallicities, causing the $[Fe/H]$ calculated via the EWs to be overestimated of a maximum of ~ 0.4 dex. This is notable from the larger dispersion towards the right end of the plot. The poor accuracy in estimating the $[Fe/H]$ for higher metallicities regime was already recognised by Battaglia et al. and later by Starkenburg et al., who

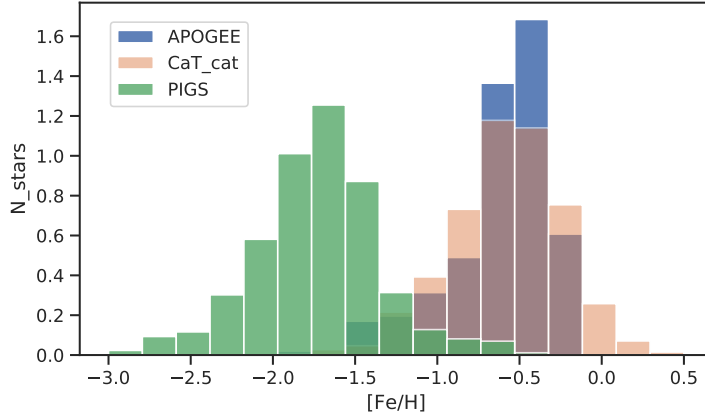


Figure 3.19 – The figure shows three different and normalized histograms that report the metallicities of APOGEE, PIGS and CaT. Looking at the peaks of the distributions, the PIGS values reflect the dominance of the MP component. On the other hand, the APOGEE and CaT samples are more MR dominated, as they are not selective in the search of the MP targets.

calibrated the CaT relation on the range $-4 < [\text{Fe}/\text{H}] < -0.5$.

To have a more complete picture, we display three histograms representing the $[\text{Fe}/\text{H}]$ distributions for PIGS, APOGEE and the CaT dataset in fig 3.19. The plot confirms a significant difference of ~ 1.1 dex between PIGS and the other two datasets. It clearly emerges that the PIGS survey is purely oriented towards the search of the most MP stars while the other two catalogues are not selective towards a specific metallicity type of star. We compute the average metallicity for each sample: $\langle [\text{Fe}/\text{H}]_{\text{PIGS}} \rangle \simeq -1.73$, $\langle [\text{Fe}/\text{H}]_{\text{APOGEE}} \rangle \simeq -0.62$ and $\langle [\text{Fe}/\text{H}]_{\text{CaT}} \rangle \simeq -0.58$ and we found that the CaT catalogues are the ones containing the highest number of MR stars. The dispersions for each catalogue are $\sigma_{\text{PIGS}} \simeq 0.39$, $\sigma_{\text{APOGEE}} \simeq 0.36$ and $\sigma_{\text{CaT}} \simeq 0.31$.

It is important to consider the fact that the metallicity-CaT formula requires passing through several steps that can be sources of uncertainties, e.g. the conversion from the *Gaia* to the V band photometry, the V_{HB} for the HB. And especially at higher metallicity, one can question the choice of fitting the CaT lines with a gaussian profile due to the dominant presence of non-gaussian wings. These effects make the match with the spectroscopic data worse for the MR stars. We need thus to keep in mind that the $\langle [\text{Fe}/\text{H}]_{\text{CaT}} \rangle$ is affected by the stars for which the metallicities derived from the CaT conversion are not very trustworthy. This is especially true for the metallicities above -0.5. In fact, if we refer to the plot 3.18, it is possible to see that for these values the difference $[\text{Fe}/\text{H}]_{\text{APOGEE}} - \langle [\text{Fe}/\text{H}]_{\text{CaT}} \rangle$ is around 0.2 and 0.3 dex, and thus this prevents us from getting completely “correct” CaT values.

Despite all the uncertainties that may derive from the application of the formula, it permits computing the $[\text{Fe}/\text{H}]$ values using the equivalent widths measurements provided by the CaT dataset. Its application is therefore a further test of the efficacy of the CaT formula on the RGB stars of dwarf galaxies. This is especially true at lower $[\text{Fe}/\text{H}]$ values, for which the results differ less from the high-resolution APOGEE

metallicities.

Thanks to the spectroscopic metallicities, we recognise as common feature of the three data samples the presence of a spread in metallicity. This spread of the $[\text{Fe}/\text{H}]$ values has been connected by many investigations to a long and rich star formation history that saw many star forming episodes resulting in different stellar populations (Newberg & Carlin (2015), Bellazzini et al. (1999)). In chapter 4 and 5 we will explore this issue in more details, trying to study separately the metal-poor and metal-rich population and comparing different theories and scenarios presented in the literature.

Chapter 4

Results

In this chapter we describe our key results derived from all the catalogues employed in this work. The main objective is the study of the Sgr metallicity distribution with a specific focus on low $[\text{Fe}/\text{H}]$ stars. We investigate the major features of the MP and MR populations trying to compare the spatial distribution of the two. To achieve this goal we use both photometry and spectroscopy. We employ the latter to enable a division between the MP and the MR sub-samples. Once the MP stars are separated from the MR ones, we examine their distributions using the PIGS photometric catalogue which has been previously cleaned by contaminators using *Gaia* data. This partition allows to elucidate the metallicity structure of Sgr and, by mapping the galaxy, it is possible to check if a metallicity gradient is present in the system.

4.1 Photometric selection

To advance in the metallicity analysis of the dwarf system, we collect all the spectroscopic $[\text{Fe}/\text{H}]$ values to create a comprehensive colour-magnitude and colour-colour diagram for the Sgr selection. The first is displayed in fig. 4.1 and gathers all the catalogues (“cleaned” to enclose only the Sgr stars) with their corresponding metallicity measurements. The CCD plays a fundamental role as it enables to divide the Sgr stellar content into two sub-populations: a MP and a MR one. This cut is performed along the y-axis (i.e. the colour) as it depicts a pronounced spread in metallicity given by the spectroscopic $[\text{Fe}/\text{H}]$ values that change moving vertically along the axis. This is due to the Ca H&K term associated to the Pristine metallicity-sensitive photometry that creates the suitable colour space to appreciate a clear metallicity gradient. The value chosen to mark the division is set at $y = 6.4$ as (see fig. 4.2a). At this value it seems reasonable to divide the Sgr population in two main groups: the more metal-poor stars, which we expect to have $[\text{Fe}/\text{H}] \lesssim -1.5$ from the more metal-rich ones, that are expected to show $[\text{Fe}/\text{H}] \gtrsim -1.5$. We are aware that it is not possible to perform a cut that enables to perfectly separate the MP from the MR objects because of the

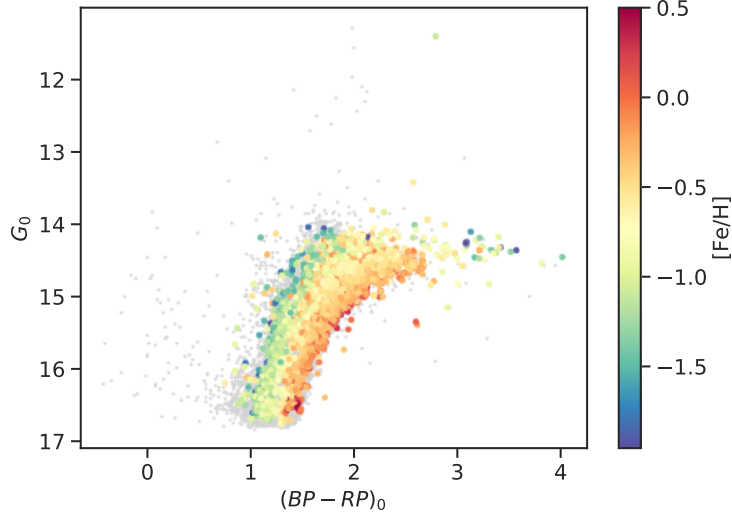
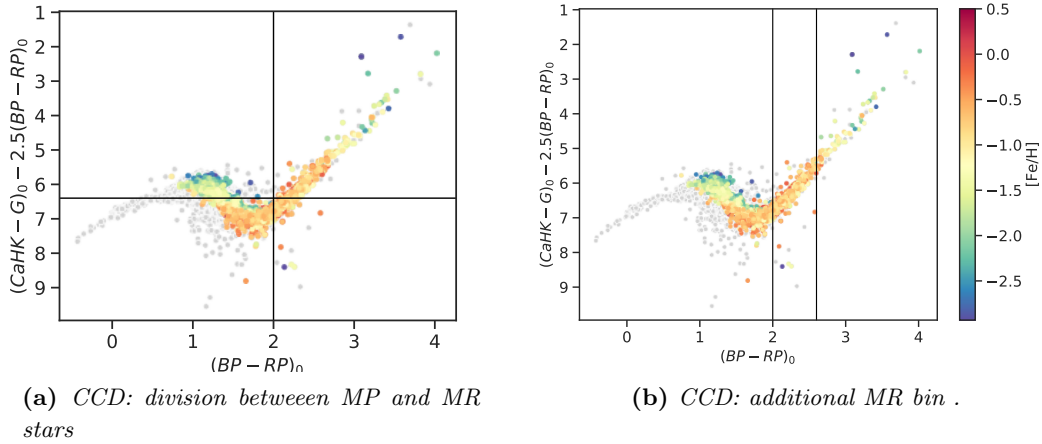


Figure 4.1 – CMD of our Sgr selection (grey dots). The spectroscopic $[Fe/H]$ are from PIGS, APOGEE and the CaT catalogues. The metallicity scale is reported on the right of the graph.



(a) CCD: division between MP and MR stars

(b) CCD: additional MR bin .

Figure 4.2 – CCDs for the Sgr footprint. **Panel a:** The CCD displays the overall Sgr sample. The horizontal black line marks the division between the MP sub-sample (top-left square) and MR stars (bottom left). The vertical line at $(BP - RP)_0 > 2$ delimits the sample of stars that are excluded from the metallicity analysis, since they are constituted mostly by AGB stars (upper right square). **Panel b:** Same CCD but showing the additional sub-group of MR stars enclosed by the two vertical lines: $2 < (BP - RP)_0 < 2.6$.

relatively high extinction in these fields. However, thanks to the Pristine photometry we first explore such division to obtain two separated pictures for the two populations. With the arrival of future Gaia data releases we foresee to be able to do a photometric metallicity estimate for this sample.

The MP stars lie above this line and consist of 6800 objects, while the MR sub-

sample is placed below and it is formed of 16017 stars. We do not consider the stars which are located in the upper right part of the CCD, limited by the vertical line at $(BP - RP)_0 = 2$, since they are mostly likely to be cold AGB or main-sequence stars on which the Pristine photometry does not work properly due to the broad molecular bands presented in their spectra. After this first election, we realize that it is possible to include more stars in the MR sub-sample with the cut illustrated by the graph 4.2b. It adds to the previous MR selection the objects enclosed between the two vertical lines at $2 < (BP - RP)_0 < 2.6$, reaching a total number of 16447 stars. Even though

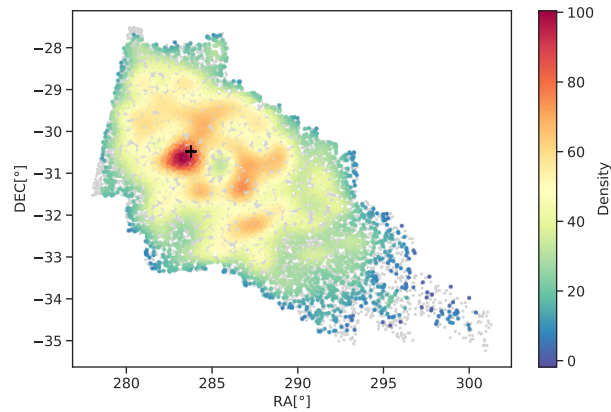
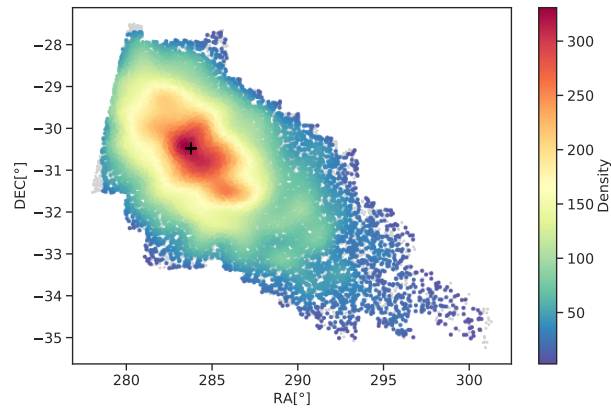
(a) *MP sub-sample*(b) *MR sub-sample*

Figure 4.3 – *Stellar density for the two MP and MR sub-samples. Panel a:* The density of the MP group plotted in RA and DEC coordinates. The black cross marks M54. **Panel b:** Stellar density of the MR populations in the same equatorial coordinates. The range of the colour bar varies for the two groups as the MP stars are largely outnumbered by the MR ones. Nevertheless, for both densities the number of objects is higher at the centre of the footprint and it declines moving toward the edges of the body.

the Ca H&K photometry does not work perfectly on the cooler stars (as we can see from the CCD where they “behave” differently from the hotter ones as the metallicity

spread is not so clear in the cooler region of the graph), we are sure that they are metal-rich thanks to the spectroscopy. Therefore it is reasonable to include them in the MR group. In this perspective, we are not comprising them based on the value of the y-axis but relying only on the $(BP-RP)$ colour. Dividing Sgr into a MP and MR sample leads to a considerable difference in the number of members belonging to these two populations, as the MP sub-samples is made up of less than half of the objects that are part of the MR population.

After having applied these cuts on the photometric catalogue with the aid of spectroscopy and after we have gone through the process of sigma-clipping the outliers at the 2 sigma level¹, we characterise the populations by assessing the mean $[\text{Fe}/\text{H}]$ in the more metal-rich and metal-poor selection. We obtain two groups: $[\text{Fe}/\text{H}]_{\text{MP}}$ with a corresponding mean value of $\langle [\text{Fe}/\text{H}]_{\text{MP}} \rangle \simeq -1.64$ and a dispersion $\sigma_{\text{MP}} \sim 0.27$, while $\langle [\text{Fe}/\text{H}]_{\text{MR}} \rangle \simeq -0.53$ and $\sigma_{\text{MR}} \sim 0.20$. After this division, the density of the stars belonging to the two populations is plotted in equatorial coordinates in the figure 4.3.

These two graphs serve to provide a rough idea of the distribution of stars in function of their metallicities. It is immediately visible that the star density is higher around the centre of Sgr where M54 lies, while moving away from the globular cluster the number of observed stars drops. Moreover, the two plots seem to suggest a shift between the centre of MP and MR samples.

4.1.1 Proper motion analysis

It has been widely recognised by many studies that Sgr shows a broad gradient in the PM values, e.g. Fritz et al. (2018); Vasiliev & Belokurov (2020). Moreover, Sagittarius has also been accounted as one of the galaxies where the PM changes more conspicuously while moving from one part of the dwarf to the other. This change has been revealed and connected by Vasiliev & Belokurov (2020) to perspective distortions created by the 3D structure of Sgr projected on the Sky rather than internal motions. The same authors recently published a new paper (Vasiliev et al., 2020) in which the study of the 3D structure and kinematics is extended also to the Sgr stellar streams. In this work (Vasiliev et al., 2020) the interaction between the LMC, Milky Way and Sagittarius is poetically depicted as a dance which involves the three systems. It is their reciprocal bonds to be responsible for a time-dependent perturbation of the gravitation potential which creates a misalignment between the stream track and the directions of the proper motions of the Sgr remnant and of its leading arm. The authors have concluded that this offset is not uniquely induced by the interactions with the MW and LMC but it is also caused by the rotation of the Sgr progenitor.

¹The sigma clipping routine calculate the standard deviation (σ) and median (m) of a distribution and remove all the points that are smaller or larger than $m \pm \alpha\sigma$ for a chosen value of α that gives the lower and upper boundary of the routine

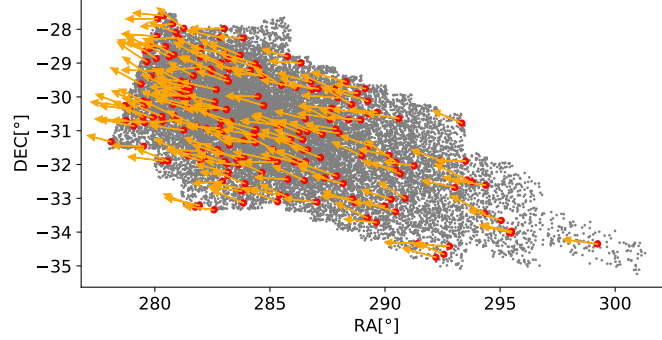


Figure 4.4 – A part of the metal-poor selection, represented by the red dots is overplotted on the photometric Sgr footprint. We choose to select randomly just 200 stars so to better appreciate the PM directions pictured by the yellow arrows. The PM measurements have been corrected from the reflex solar motion. It is evident that the direction of the arrows seem to be quite well lined up with the elongation of the Sgr body, which itself coincides with the orbital direction.

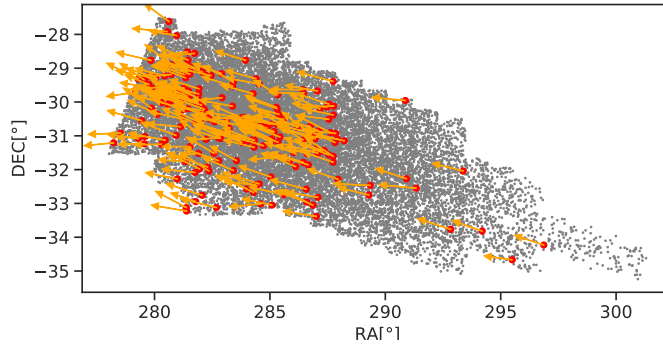


Figure 4.5 – This plot shows the same quantities and follows the same procedure used for producing the fig.4.4. In this case the Sgr metal-rich selection is represented. The alignment observed for the MP sample (just with few degrees off, especially at the outer areas) is also visible for this group of star.

To have a deeper insight on our Sgr selection, we analyse the proper motion of the two MP and MR populations. We are particularly interested to see if we can spot any evident internal difference between the stellar groups. Firstly, for both samples, it is necessary to correct the PM data of the constituent stars for the solar reflex motion. Using the *gala* library (Price-Whelan, 2017), we correct the PM of the Sgr stars “cleaning” it from the effects induced by the solar motion. We compute for Sgr the mean PM values in equatorial coordinates and compare them with the ones presented in the *Gaia* DR2 proper motions paper (Fritz et al., 2018). The results calculated for our Sgr selection are for the component in right ascension $\mu_{\alpha}^* \simeq -2.68 \text{ mas yr}^{-1}$ and for the declination component $\mu_{\delta} \simeq -1.39 \text{ mas yr}^{-1}$. They seem to be compatible with the *Gaia* ones where $\mu_{\alpha}^* \simeq -2.74 \text{ mas yr}^{-1}$ and $\mu_{\delta} \simeq -1.36 \text{ mas yr}^{-1}$. After the correction for the solar motion, we plot the two MP and MR footprints

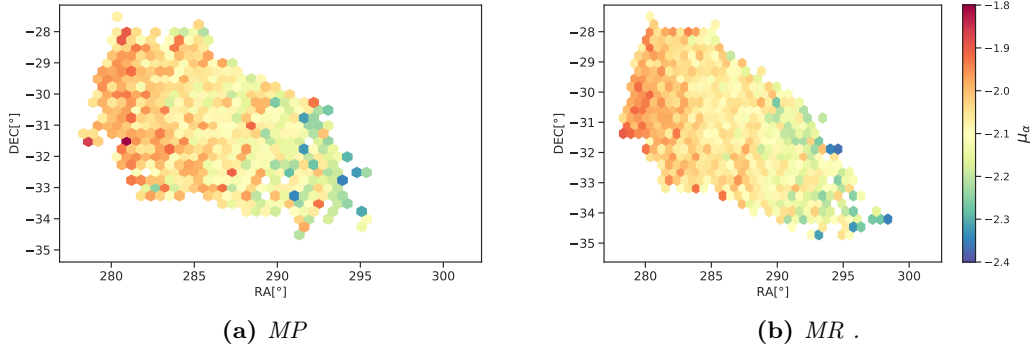


Figure 4.6 – *Sgr footprint in equatorial coordinates colour-coded by μ_α^* , corrected for reflex solar motion. **Panel a:** The MP pop. displayed in the same PM scale used for the MR sub-sample **Panel b:** MR stars divided in the same PM bins used for the MP group.*

(fig.4.4 and 4.5) in which the arrows depict the corresponding PM directions. The

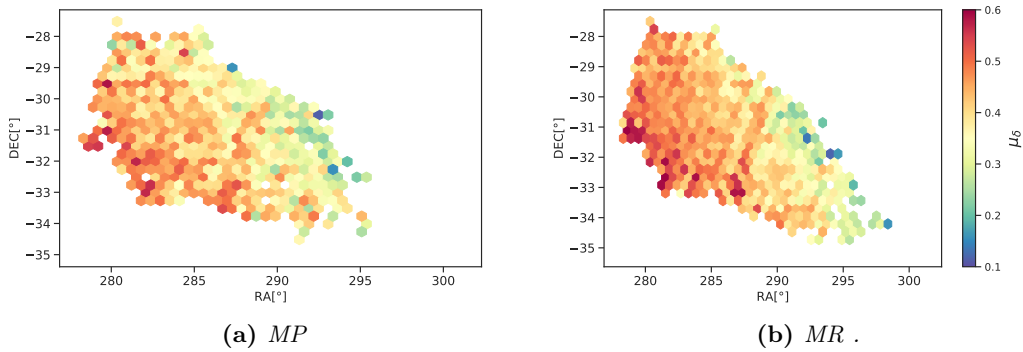


Figure 4.7 – *Sgr footprint in equatorial coordinates colour-coded by μ_δ . Same procedure adopted for the fig. 4.6 **Panel a:** MP stars displayed in the same PM scale used for the MR sub-sample **Panel b:** MR stars divided in PM bins and colour-coded by the δ component of the PM.*

resulting graphs suggest that, looking at the Sgr main body, the offset between the PM and the apparent direction of motion of the dwarf galaxy is not so noticeable. It seems that, despite a possible but small offset (that may be not so visible as we are selecting a random sample of Sgr stars), there is an alignment between the major axis of the body and the PM directions. This result is in agreement with the findings of many authors reported in section 2.4, who assent about the fact that the orbit of Sgr and the elongation of its body are lined up with the direction of motion. Additionally, the two populations do not manifest any meaningful difference in their internal motion and structure, as the arrows have the same direction for both the MP and MR selections. To proceed in this analysis, we plot the Sgr footprint in right ascension and declination coordinates and colour-coded it by the PM values. For both right ascension and declination we compare the two populations so to be able to detect any differences

in the internal structures. Looking at the results in figures 4.6 and 4.7, no obvious difference emerges: for the α component the PM values increase moving towards the Galactic centre ($RA \approx 266^\circ$ & $DEC \approx -28.9^\circ$, from the SIMBAD catalogue Wenger et al. (2000)), meaning towards lower RA and DEC values, fig.4.6a.

A similar trend appears for the declination component, which shows higher value moving to the right part of the graphs 4.7b, thus towards lower RA. However, for μ_δ the values are slightly enhanced for lower DEC. Again, despite this different aspect, the plots do not exhibit any substantial differences between the two populations, meaning that the global movement of the two stellar groups is quite similar.

4.2 Metallicity distribution

To have a deeper insight in the metallicity distribution of Sgr we create a 2D histogram (fig. 4.8) displaying the ratio between the MP and MR stars selected via the photometric cuts conceived in section 4.1. The ratio is represented in the binned right ascension and declination space and it aims to spot the changes in the metallicity pattern while moving along the Sgr body. The histogram suggests that the relative

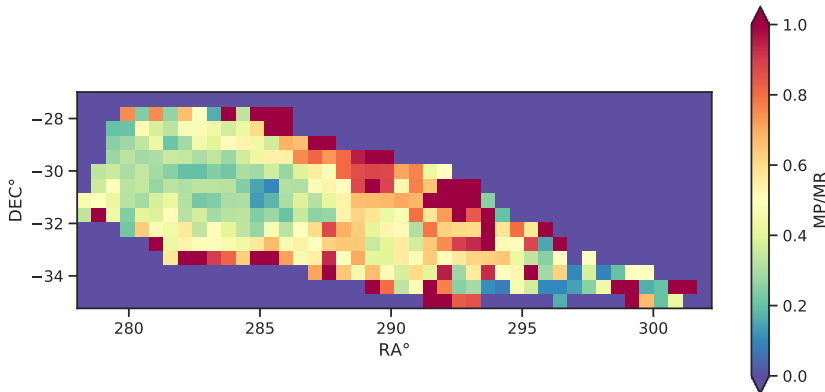


Figure 4.8 – 2D histogram of the ratios MP/MR plotted in RA and DEC space. The space is divided in bins of 0.55° each colour-coded by the ratios values. To have a clear spread in colours, the values $MP/MR > 1$ are coloured as the $MP/MR = 1$.

fraction of MP stars is higher at the edges of the main body of Sgr. In effect the central area shows on average a rather low fraction of MP stars while proceeding towards the borders we can see the ratio increasing. It seems reasonable to advance the idea that later star forming episodes, taking place close the centre, may have led to a metallicity enrichment in the successive generations and thus leading to a more MR population formed on top of a more distributed MP one. Therefore, MR star forming episodes occurring at the centre only, can explain the metallicity gradient shown by the dwarf system. In addition, more centrally MR components can also justify the presence of

a metallicity gradient along the Sgr stream as they made, throughout the existence of the system, its tails more metal-poor. To gain a more clear picture of this issue, we compare our findings with the results presented in the literature (section 5.1).

4.2.1 Concentric distribution

To look deeper into the metallicity distribution of Sgr we decide to divide it in several parts so to examine the relative metallicity distribution for each region of the main body. Inspired by the idea of Mucciarelli et al. (2017), who mapped the change of metallicity in function of the projected distance from the Sgr centre, we decided to cut our Sgr stellar sample into concentric annuli as shown in the plot 4.9. In this way it is possible to analyse the metallicity for each annulus. However, we have considerably enlarged the area analysed, since the region considered by Mucciarelli et al. covers only $\sim 70^\circ$ around the Sgr centre.

The equation adopted for the division is the simple equation of a circle, whose centre corresponds to the GC M54: $(RA - RA_{M54})^2 + (DEC - DEC_{M54})^2 < r^2$.

The radius of each ring increases with a step of 1.5° and, starting from the very central region, the coverage reaches the outskirts of the main body (see fig.4.9). Although the division into concentric rings with the same radius maintains a geometric and spatial symmetry, we can see that the stellar density in outer regions of Sgr is considerably lower with respect to the central areas. Therefore it is likely that the difference in the number of stars for each annulus is rather big and it may affect the analysis. Despite this, for describing the change in metallicity of the annuli we create the plot shown in fig.4.10, which provides the variation of the MP/MR ratios moving away from M54. The errors are calculated assuming a poissonian distribution, even if we are aware that this assumption is not the perfect option as its validity can break due to the non total independence of the MP and MR measurements. Moreover, as was foreseeable, the error bars become bigger with larger distances from the centre, as the lower numbers of observed stars in the non central areas make the results less statistically robust. Another cause is the higher contamination from the MW stars in the exterior areas. As a matter of fact the proper motion changes moving across the Sgr body, thus it is probable that we are considering more MW stars as the proper motion selection conceived for the centre breaks down at the edges of the body.

In order to better clarify this issue, we check if the Sgr over-density for the stars selected for each annulus has moved in proper motion space. We produce several plots representing the different groups of stars in PM space (see Appendix A). They seem to indicate that the the PM condition is not longer valid for the external areas of Sgr. This effect added to the low numbers of data points contained in the last rings can explain the enlargement of the error bars moving away from the Sgr centre. Notwithstanding these uncertainties, the trend displayed in the plot suggests that the ratio rises as the distance from M54 grows. This feature would confirm the result seen in the 2D histogram 4.8, which also reveals a relative higher fraction of MP stars at

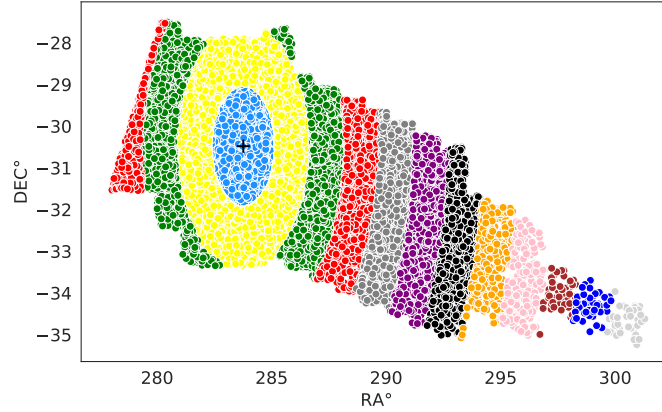


Figure 4.9 – Division of Sgr dSph in concentric annuli (differentiated by different colours). As usual, M54 is represent by the cross symbol. The radii increase with steps of 1.5° and cover almost the entire Sgr footprint. There is just a tiny part which is not covered (grey part) as the few data from this region (especially regarding the MP component) do not allow a reasonable statistical analysis. The circular symmetry is not entirely visible as the x and y scales are different.

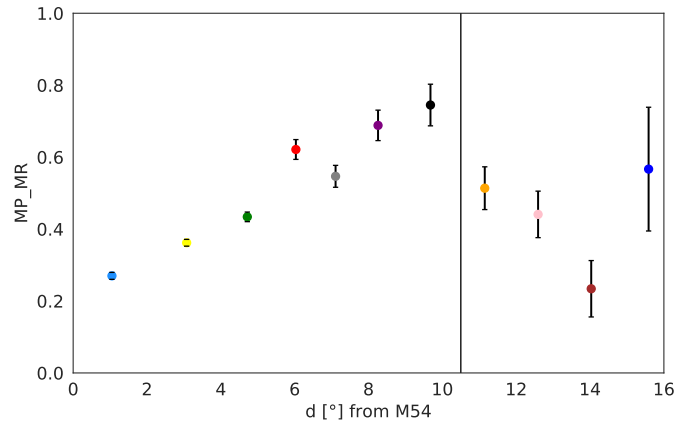


Figure 4.10 – The ratios of MP/MR stars calculated for each annulus. The x -axis represents the distance in degree from the position of the GC M54 which is implemented adding 1.5° to the middle point of the previous annulus. The points are calculated and connected to the respective ring shown in fig.4.9 of the same colour. The black vertical line marks the beginning of the most contaminated part of Sgr as it can be seen from the increasing size of the error bars.

the edges of the dwarf main body.

Trying to increase the “resolution” in the inner regions we create smaller bins and we combine the outer rings. To this aim we slightly change the size of the concentric annuli: fig.4.11. With this new configuration we aim to diminish the wide difference between the statistics of the rings so to reduce the error bars of the ratios MP/MR.

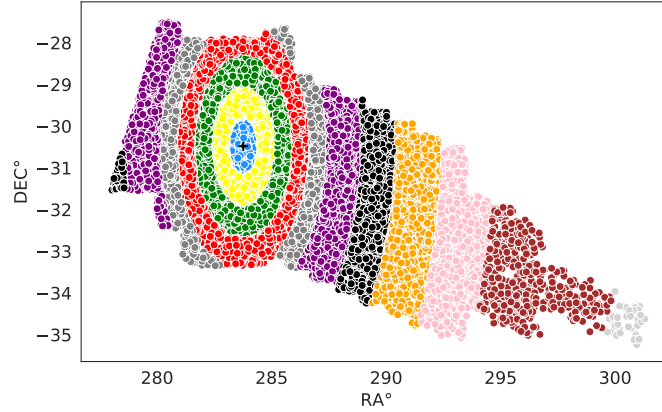


Figure 4.11 – *Division of Sgr dSph in a diverse concentric partition. M54 is identified with the cross symbol. The radius no longer increases smoothly but its growth guarantees that the number of stars is not too different from one region to the other. Again, the circular shape of the division is not directly noticeable due to the different scales of the horizontal and vertical axis.*

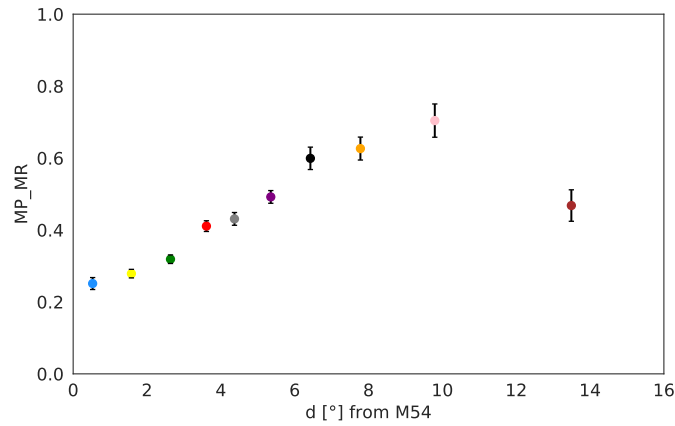


Figure 4.12 – *The ratios of MP/MR stars calculated for the new concentric division. Again the colour of each point is linked to the corresponding annulus. The trend shown in the present graph confirms even more markedly a rise of the relative ratio of the MP stars while moving towards the edges of Sgr. The distances for each ring are calculated from the centre of Sgr, which corresponds to M54.*

This improvement is displayed in the plot 4.12. In this latter, the radius does not longer increase regularly but its change is aimed to guarantee a more uniform partition of the data among the rings. that results in smaller error bars.

4.2.2 Elliptical distribution

To further test this issue, we divide our sample in an even different configuration. Indeed, by observing the 2D histogram (4.8), we are led to believe that an elliptical division could be more suitable for the metallicity pattern shown by the graph. We

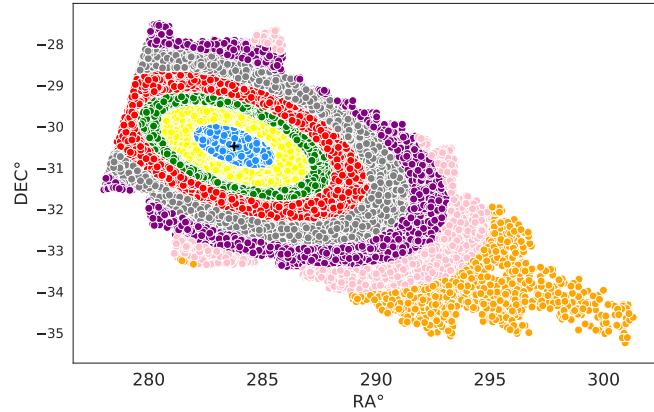


Figure 4.13 – *Division of Sgr dSph in concentric ellipses centred around M54. The parametrisation of each ellipse varies in order to enclose the similar number of objects for each subdivision.*

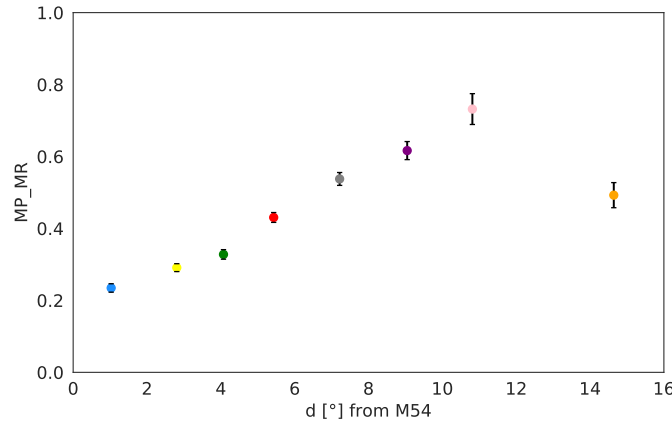


Figure 4.14 – *The ratios of MP/MR stars calculated for the elliptical partition. It is possible to observe that moving far from the centre the ratios growth until the last ellipse for which the MP/MR quantity suddenly drops. The error bars are calculated assuming a Poissonian distribution and the colours of the points indicate the corresponding division in the plot 4.13. Also for this plot the distances are taken respect to the position of M54.*

thus modify the circle equation into the one of a rotated ellipse:

$$\frac{(RA - RA_{M54})^2}{a} + \frac{(DEC - DEC_{M54})^2}{b} + c \times (RA - RA_{M54}) \times (DEC - DEC_{M54}) < r^2 \quad (4.1)$$

Again we use as centre the coordinates of M54, a and b indicate the semi-major and semi-minor axis while c describes the inclination angle between the ellipse and the major axis. The resulting partition is depicted in the graph 4.13.

We follow the same procedure used for the annuli to analyse the metallicity distribution within the various ellipses. The plot 4.14 is the outcome of this analysis. The trend shown is quite similar to one attained with the previous division. The relative ratio grows in the outer regions and drops promptly for the last ellipse. The problem of having little data for the last regions also persists in this new division as we can see from the error bars increasing with the distance from the centre. However, this new approach reinforces the idea of a rise of the relative ratio of MP stars at the edges of the body of the galaxy and provides a further hint for the study of its metallicity distribution.

4.3 Variation of the spatial density vs. metallicity

To advance our knowledge about the spatial distribution of different $[\text{Fe}/\text{H}]$ star groups in Sgr, we choose to explore the variation of the stellar density in function of metallicity. We try therefore different cuts for the metal-poor stars to further study their spatial information (see plot 4.15). For each selection we plot in equatorial coordinates the stellar density and we compute the mean $[\text{Fe}/\text{H}]$ and their dispersion

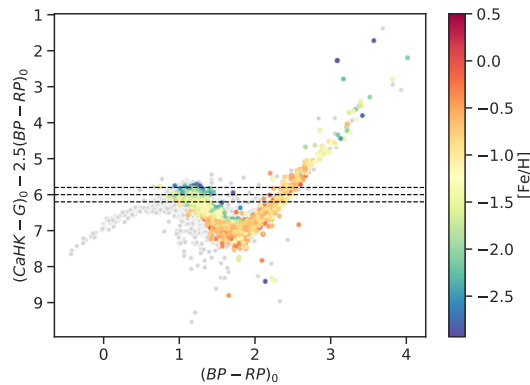


Figure 4.15 – *CCD for Sgr colour-coded by the spectroscopic $[\text{Fe}/\text{H}]$ values. The horizontal dashed lines mark the different cuts along the colour axis perform to investigate the spatial distribution of the MP population. The values adopted are $y = 5.8, 6, 6.2$*

with the sigma clipping routine. The plots are shown in fig.4.16 .

Concerning the MP population, we notice that until the cut at $y = 6$ the density peaks around the central area which can also be identified thanks to the presence of M54. The corresponding metallicity to this limit is $\langle [\text{Fe}/\text{H}] \rangle \sim -1.68$, with a dispersion of $\sigma \sim 0.17$. Nevertheless, it is possible to see that there are also other - even if smaller - overdensities at lower right ascensions (especially around $\text{RA} \sim 280^\circ$). Above $y = 6$ the pattern of the density is still more defined as the stars are densely clustered

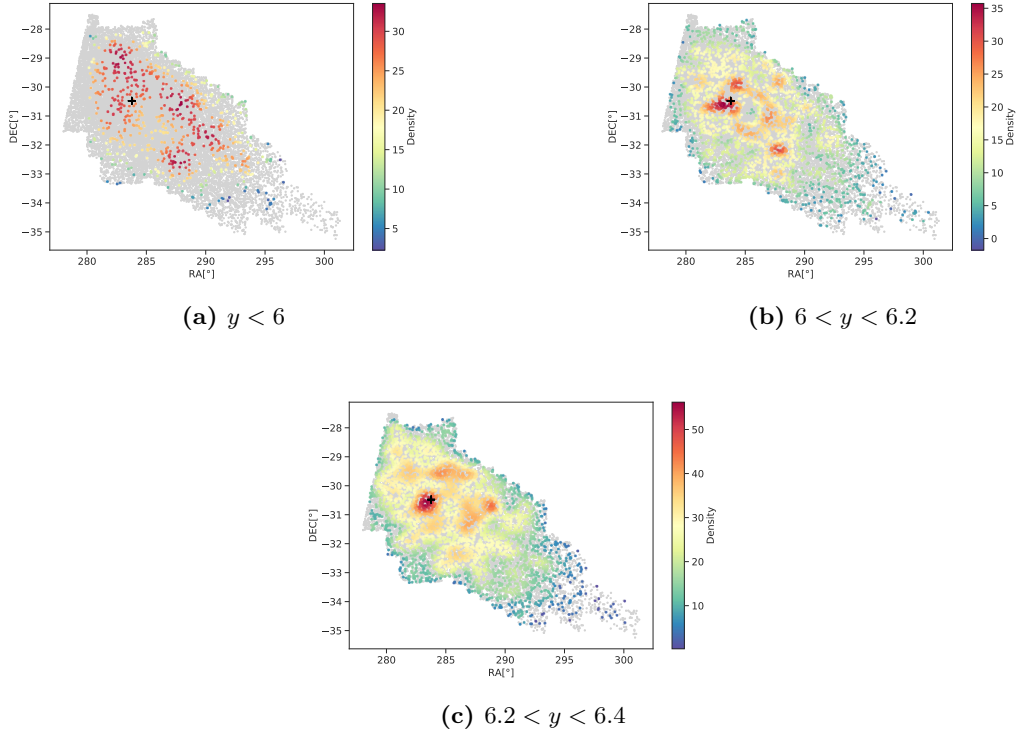


Figure 4.16 – The Sgr footprint with the stellar densities calculated for each cut applied on the CCD of the MP population (4.15). In all plots M54 is depicted with a black cross and identifies the Sgr centre. **Panel a:** MP star sample laying below $y < 6$. No clear pattern in the spatial distribution is visible, but the stars are quite homogeneously distributed all over the Sgr body. **Panel b:** Stars included in the range $6.0 < y < 6.2$. It is visible that the overdensity is spreading around the globular cluster and at $RA \sim 280^\circ$. **Panel c:** The more populated MP sub-sample falls within the range $6.2 < y < 6.4$. Also in this last case, the density is clearly higher around the GC where it has its peaks and it drops moving far away from the centre. However, again at $RA \sim 280^\circ$ the MP objects are clustered together constituting a smaller stellar overdensity.

around the GC. Corresponding to a “higher” cut in the y-axis, these stars possess a mean metallicity greater than the previous group. The mean value is around -1.33 while the dispersion is ~ 0.11 . Below $y = 6$ no clear feature is noticeable in the spatial distribution of these more MP objects that have $\langle [Fe/H] \rangle \sim -1.92$ and $\sigma \sim 0.24$. In general, the more MP stars are not creating any specific density pattern for very low $[Fe/H]$ values. To further investigate this aspect we look at the spatial distribution of the Sgr VMP stars in the following section 4.3.1.

4.3.1 Insight on the VMP

Since it has been already shown that Sgr galaxy hosts a very metal-poor stellar populations (Chiti & Frebel, 2019), we choose to look deeper among the selected MP

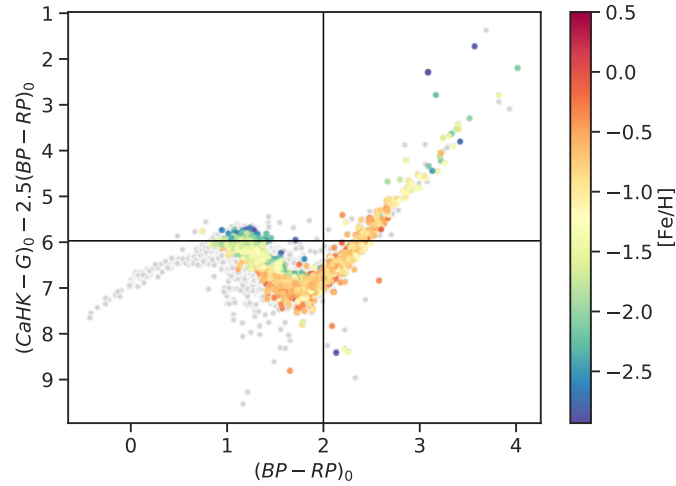


Figure 4.17 – CCD of the Sgr footprint. The selected VMP stars are enclosed in the left top box marked by the continuous black lines. The metallicity scale allows to approximately cut at a y value (see the vertical black line) which roughly corresponds to $[Fe/H] < -2$.

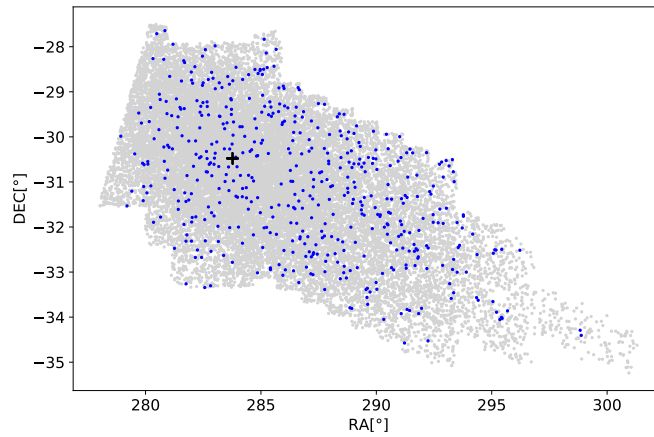


Figure 4.18 – The VMP sub-sample (in blue) is overlapped with the Sgr footprint plotted in equatorial coordinates (in gray). The VMPs are extended quite uniformly over the dwarf galaxy. Their number is slightly higher around the position of M54 where in general the stellar density is greater.

group trying to isolate a VMP sub-component.

To this purpose we use the CCD illustrated in Fig.4.2 to apply a new photometric cut that isolates as best as possible the spectroscopically confirmed Sgr stars with $[Fe/H] < -2$. The cut is shown in fig. 4.17 and it is located at $y = 5.97$. It is clear that the cut in the colour space does not enable to include uniquely VMP stars as it is likely that also less MP objects fall into this partition. However, to better verify the elected division and to get more metallicity information we employ again the sigma clipping routine and we derive $\langle [Fe/H]_{VMP} \rangle \simeq -2.09$ and $\sigma_{VMP} \simeq 0.21$.

We then follow the same procedure used for the MP and MR samples: we plot in space the VMP group to see how it spreads over the Sgr footprint. This is visible in the graph 4.18 in which it is possible to observe the VMP objects covering homogeneously the main body of Sgr. The absence of a specific pattern in their distribution has been already discovered in the analysis presented in the previous section 4.3 with the isolation of the sub-sample at $y < 6$. The uniform distribution of VMPs suggests that no such stars were formed recently in the more inner area and their mixing can be linked to the gradual disruption of the old progenitor which has just left the wider stellar tails and the former nucleus now constituting the Sgr dSph system.

4.4 Age of VMP stars in Sgr

To explore deeper the Sgr system, we couple the metallicity information collected so far with the study on the age of the VMP population to check if our selection shows an age that is consistent with the result presented in literature. To this end, we made use of isochrones and over plot them on our CMD. Since we do not have data for all the stellar evolution stages, for instance we miss the old main-sequence turn-off point, we limit this analysis to the red giant branch region.

We use the MIST models (Dotter, 2016) selecting the isochrones suitable for our VMP population. The average $[\text{Fe}/\text{H}]$ of the VMP population is -2.0. The MIST isochrone models assume $[\alpha/\text{Fe}] = 0.0$, but typical VMP stars usually have $[\alpha/\text{Fe}] = +0.4$. We therefore calculate which overall metallicity is best for the isochrones using the following equation:

$$Z_{\text{H}} = [\text{Fe}/\text{H}] + \log_{10}(0.661 \times 10^{[\alpha/\text{Fe}]} + 0.339) \quad (4.2)$$

Inserting the observed $[\text{Fe}/\text{H}]$ as -2.0 and $[\alpha/\text{Fe}] = +0.4$ (Carretta et al., 2010), the isochrone metallicity results ~ -1.7 . We use the theoretical *Gaia* photometry isochrones and for all models the photometry is dereddened.

We check an age range from 2 to 13 Gyr and we shift the corresponding isochrones for the distance modulus of Sgr, for which we assume $D = 26.4$ kpc (Ferguson & Strigari, 2020). The results are illustrated in panel ???. Even if it is difficult to discriminate between older ages (i.e. 10-12-13 Gyr), it is clear that younger ages (2-4-6 Gyr) and intermediate-age (8 Gyr), being shifted from the data, constitute a worse model for the VMP sample. At this phase of the work, we are not quantifying the goodness of the fit, but we restrict our analysis to investigate the age of VMP population and to a following comparison with other studies. In a future stage of the project it could be very interesting and informative to establish some criteria to decide which isochrone fits best to the data and also to compare the ages of the more metal-poor stars with those of the more metal-rich stars.

Despite this “lack”, our findings are in agreement with the scenarios delineated in the majority of studies about the Sgr stellar populations (Monaco et al. (2003); Siegel et al. (2007)), mostly indicating that the metal-poor stars are aged > 10 Gyr, and the VMP

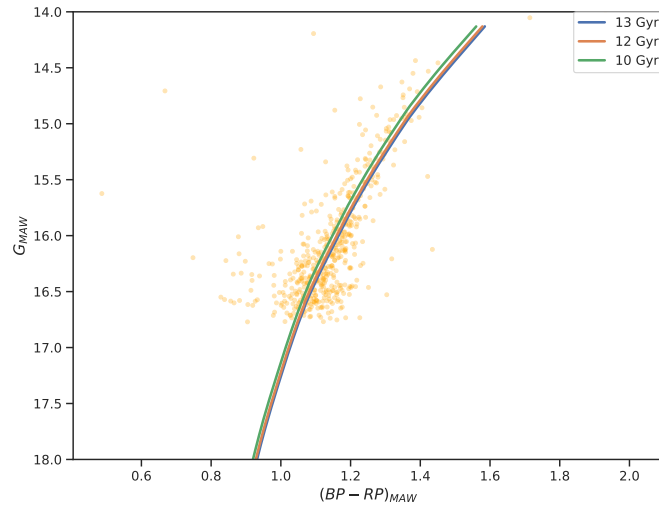


Figure 4.19 – Old MIST isochrones created with Gaia photometry and shifted to the distance modulus of Sgr dSph and over plotted on the Sgr VMP selection (orange dots), whose photometry has been dereddened. The different age of each isochrone is reported in the legend.

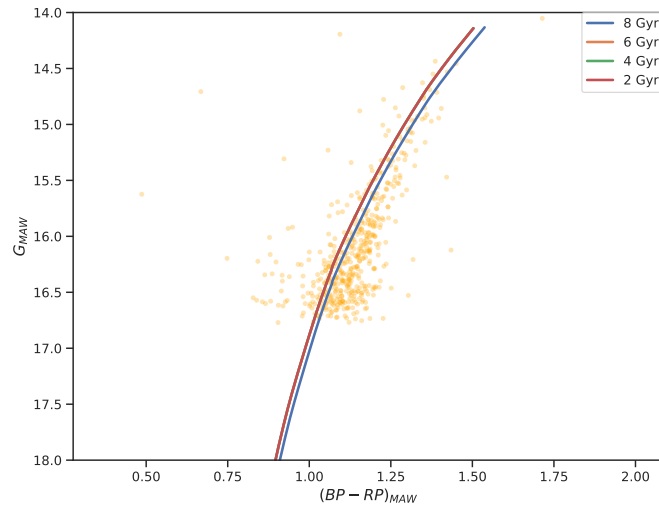


Figure 4.20 – Intermediate-age and young MIST isochrones created following the same procedure adopted for the models reported in 4.19.

ones are found to be ~ 13 Gyr. For our analysis, it is also reasonable to find an age for the VMPs older than the Sgr infall, which occurred ~ 5 Gyr ago (Ruiz-Lara et al., 2020). This might point to the idea that a stellar mixing between the old and MP and stars of different $[\text{Fe}/\text{H}]$ and ages occurred as a consequence of the deep infall of Sgr onto the MW disk.

4.5 Outline of the main findings

The main outcomes achieved by the analysis performed have been possible thanks to the Pristine metallicity-sensitive photometry. Indeed, this study has revealed the effectiveness of this technique on dwarf systems such as Sgr. Indeed, using the Pristine colour space we were able to distinguish the more metal poor stars from the more metal rich ones. This is an additional proof of the validity and power of this method on systems for which the spectroscopic data are lacking or incomplete.

Proceeding in the metallicity analysis, we found that the relative fraction of MP stars seems to be higher at the edges of the main body of the dwarf satellite. To attain this conclusion, we started dividing the two populations and plotted their spatial distributions (see fig.4.3a, 4.3b). We applied the photometric cuts with the help of the spectroscopic data sets that enabled us to roughly separate the MP from the MR component. We computed the ratios between the MP and MR selections and we examined its variation in space. Initially we use a 2D histogram (fig.4.8) and later we studied the ratios for different Sgr divisions: both circular and elliptical (fig.4.10, 4.12 and 4.14). Thanks to this investigation we have been able to unearth a particular aspect in Sgr dSph. As a matter of fact, a clear rise of this quantity does appear until the very outer regions of the galaxy. Regrettably, in the outer areas of Sgr, the numbers of data are so low that the statistics are not longer reliable and this is clearly visible in the error bars increasing moving towards the Sgr edges.

A part of the analysis concerning the MP and MR populations has also been dedicated to the study of their proper motions. Especially, we tried to spot any substantial difference in the internal kinematic of the Sgr system. However, our analysis has not reveal any difference concerning the PM of the more metal-rich and metal-poor selections. On the other hand, it seems to agree with other studies (Ibata (1999), Vasiliev & Belokurov (2020)) that found an alignment between the direction of the proper motion of the stars and the orientation of the Sgr remnant.

As further step, we compared the variation of the stellar density of the more metal poor stars attempting to discover at which metallicities the spatial distribution shows peaks or overdensities. We found results that have unveiled a marked higher central distribution which shades for the lower $[\text{Fe}/\text{H}]$ group, leaving space to a more homogeneous stellar distribution. We paid a special consideration to the VMP stars. We singled out this sample applying again a photometric cut in the CCD, as depicted in fig.4.17. After having plot the desired selection in equatorial space (fig.4.18), it is possible to see that the stars seem to be uniformly distributed along the Sgr body. To study deeper the VMP selection we then employed the MIST models for isochrones to assign an age to this group of stars which result to be older than 10 Gyr.

Chapter 5

Discussion

In the following chapter we provide different interpretations of the scientific results concerning the metallicity distribution of the Sgr galaxy. By comparing the outcomes of our research with the results of previous studies, we intend to contextualize our work and connect it to the on-going study and research of the most metal-poor stars around the Milky Way Galaxy. Also, it allows us to give further justification to our conclusion that there is a metallicity gradient in Sgr dSph. Thus giving a more complete picture of the galaxy and shedding light about its evolution before and after the interaction with the MW.

5.1 Comparison with literature

Several studies (e.g. Newberg & Carlin (2015); Mucciarelli et al. (2017)) have already pointed out the idea that the metallicity gradient undeniably present in Sgr dSph may correspond to an age gradient that predicts recent metal-rich bursts taking place closer to the centre of Sgr. For example, Mucciarelli et al., by considering the central region of Sgr dSph (generally named as “Sgr,N”), analysed the chemical abundances of the stars belonging to the GC M54 and to Sgr,N and tried to lessen the contamination by Galactic foreground stars. They studied the metallicity distribution of this restricted stellar sample by dividing it into different radial annuli. Their analysis revealed a prominent metallicity gradient, which shows a variation in the peak of the metal-rich population following the projected distance from the centre of the nucleus of Sgr. Even though their stellar sample is considerably more restricted than ours (they just look at a region of $\sim 70 \text{ pc} \simeq 0.15^\circ$ from the centre), they arrived to a conclusion that seems to be in accordance with our outcome: the more metal-rich population dominates the innermost region while the metal-poor component becomes more important at larger radii. This variation of the iron content within the system has been linked to an age gradient which in turn can be explained by various metal-rich bursts that saw later stellar generations being more concentrated in the proximity of

the centre of the system. To explain the metallicity trend, Mucciarelli et al. resort to a decisive stripping event that started 7.5 Gyr ago when Sgr accomplished its first peri-Galactic passage and finished about 2.5 Gyr ago. This violent process would have basically removed all the gas in the system preventing other star formation episodes. Already in 1998 evidences of a strong metallicity gradient were provided by Bellazzini et al. Thanks to the first photometric results of the Sagittarius Dwarf Galaxy Survey (SDGS), the authors derived a radial spread from $[\text{Fe}/\text{H}] \sim -1.5$ to $[\text{Fe}/\text{H}] \sim -0.7$ and revealed a more metal rich stellar population dominating the central region of the galaxy. In the second paper released by the SDGS, the metallicity range was extended to a limit of $[\text{Fe}/\text{H}] \sim -2.1$ and about 60% of the stellar budget was estimated to be metal-rich (Bellazzini et al., 1999). This span has also been related to a significant age variation in the dwarf system caused by a protracted star formation history that shows the peak of star bursts around 8-10 Gyr ago when $-1.3 < [\text{Fe}/\text{H}] < -0.7$. Both studies had to deal with the difficulty of separating in the very central area the more metal-rich stars belonging to Sgr,N from the overwhelming presence of stars from the old GC M54. In a more recent study of 2008, Bellazzini et al. managed to divide the star members of Sgr,N from the old SP belonging to M54 thanks to metallicity information and using their different radial velocity profiles. They claimed that the $[\text{Fe}/\text{H}]$ values follow a broad distribution which peaks around $[\text{Fe}/\text{H}] \sim -0.4$ and spans from $[\text{Fe}/\text{H}] \gtrsim -1.0$ to super-solar metallicities. Moreover, they verified that the nucleus of Sgr is mainly dominated by an intermediate-age and metal-rich population.

In a study conducted as part of the ACS Survey in 2007, Siegel et al., using the Hubble Space Telescope photometry, were able to detect the presence of multiple SPs in the disrupting system of Sgr. Although it represents a clear minority, a MP ($[\text{Fe}/\text{H}] \sim -1.3$) and old (10 - 11 Gyr) stellar component resides in Sgr,N. Nevertheless, the predominant groups were found to be intermediate-age (5 - 8 Gyr) and ranging in the MR regime ($-0.7 < [\text{Fe}/\text{H}] < -0.4$). Once more, this heterogeneous and richly populated panorama is traced back to multiple star bursts occurring over the entire existence of the dwarf that cause an evident metallicity gradient in the system, in which the most metal rich objects were born closer in.

Another interesting idea is contained in a recent paper published by Johnson et al. (2020). Shifting the focus from the main body to the wide stellar streams of Sgr, the authors identified a wide range in $[\text{Fe}/\text{H}]$ from ~ -0.2 to ~ -3.0 where the variation in metallicity is found to be kinematically dependent. The MP stars (with $[\text{Fe}/\text{H}] < -0.8$ down to -2.0) are considerably hotter, kinematically speaking with respect to the more MR stars, thus the two components have been set apart and studied separately. They also explored the possibility that this MP and kinematically-diffused component was in the past the stellar halo of Sgr. In this scenario, because of the interaction with the MW, this outer component had been stripped away, causing the MP stars to be removed from the progenitor before the colder MR part. Many hypotheses are discussed for the origin of stellar halos in dwarfs (e.g. disk outflows, stellar feedbacks or cold stellar wraps that were stripped away from the progenitor and subsequently

diffused and reheated), but the formation processes behind remain still unclear.

The increase of more metal-poor stars at the outskirts of this galaxy may be compared with the metallicity distribution of the MW halo. As a matter of fact, Youakim et al. (2020) used a sub-sample of MW (inner) halo stars from the Pristine survey and, analysing their metallicity distribution, showed a decrease of metallicity with increasing heliocentric distance. The metallicity-distribution function (MDF) presented for these halo stars peaks at $[\text{Fe}/\text{H}] -1.6$, which appears to be more metal poor than the Sgr core as we derived in our analysis a peak at $[\text{Fe}/\text{H}] \sim -0.69$. This value is about 2 dex higher than the mean metallicity value reported in the literature (that is ~ -0.5 dex as discussed in sect.2.5). This difference is probably due to the contribution of the PIGS metallicities. Moreover, the MDF found for the MW halo matches with a closed-box chemical enrichment model (Youakim et al., 2020), while for Sgr the chemical evolution is better described by a leaky-box model (McWilliam et al., 2013), which is very similar to the close model but it takes into account the effects of outflows of gas from the galaxy. However, these two models seem to predict the same metallicity distribution (Tremonti et al., 2004), with the only difference that in the leaky model the gas outflows play a major role in the chemical enrichment of the galaxy. This latter is the case for Sgr, for which it has been shown (McWilliam et al., 2013) that despite its overall metal-rich composition, the elements produced by more metal-poor stars dominate the chemical panorama of the galaxy.

Another question of great importance that is still unsolved concerns the formation of M54 and its connection with the metallicity distribution of the Sgr system. It is in fact compelling at this point to question if this overdensity, seen around the globular cluster, may be identified as the mass-seed which leads to the assembly of the more MR Sgr dSph nucleus. Indeed, as we already commented in sect. 2.2.1, it has been demonstrated (Bellazzini et al., 2008) that Sgr is a nucleated galaxy whose nucleus coincides in position with the old and MP GC M54. This latter, driven by dynamical friction, could have fallen into the central potential well of Sgr galaxy ending up on top of the already present MR Sgr nucleus. Despite the cut that we applied on the very central area of Sgr, this mix between the two populations affects also our Sgr selection.

In this work, we extend the analysis of the metallicity gradients in the Sgr galaxy out to larger radii, reaching a distance of about 17° from the centre (for which we assume M54) and we use an unprecedented large sample of stars in this analysis, a MP sample ($\langle [\text{Fe}/\text{H}] \rangle \sim -1.64$) of 6800 and a MR sample ($\langle [\text{Fe}/\text{H}] \rangle \sim -0.53$) of 16447 objects. Notwithstanding the risk that the metallicity distribution of Sgr dSph is biased by the GC M54, its presence affects only the inner $1-2^\circ$ from the nucleus. However, a complete unbiased metallicity distribution of Sgr dSph in the very central areas is still missing.

Despite all these factors, we are still able to appreciate an increasing growth of the MP/MR ratio moving towards the edges of the dwarf. This is possible even if the number of observed stars is markedly higher around M54, and probably contaminated by the same. Furthermore, a more central concentration of younger and MR stars is a

feature shared also by other dSph galaxies not only in the Local Group. For instance, in a recent investigation about the properties of the dSph satellites in the Cen A group (Müller et al., 2020), 12 samples of dwarf galaxies have been found to host younger (~ 300 Myr) and more MR stars in the centre. This is also true for the Fornax galaxy, with which we will carry out a more detailed comparison in the section 5.1.1 due to its similarity with Sgr.

After taking into consideration all these investigations, we expect that the existence of a metallicity gradient is a typical signature of the dwarf galaxy. We moreover note that our results are based on one (rather) homogeneous sample of stars - the PIGS photometric sample - all selected in a very similar way across the whole footprint of the Sgr dSph. The spectroscopic datasets used to inform us where MP and MR stars are located in colour-colour space were more inhomogeneous, but taken together they span the whole metallicity range.

Focusing on the study of the distribution of the very metal poor stars, we arrived to the conclusion that these objects are homogeneously distributed within the Sgr main body. As a consequence they seem to be well mixed with stars that have different metallicities.

Lastly, an interesting comparison with a recent study about the Sgr systems concerns the proper motion of the galaxy. By studying the PM of our MP and MR selection in the remnant (sect. 4.1.1), we found for both samples an alignment between the PM direction and the elongation of the Sgr body. This result is also presented in the papers of Vasiliev et al. (2020) (even if they do not set their analysis for separated metallicities). However, as the Sgr system presents a solid rotation, the corrections needed to be applied on its motion are likely to be more complicated than the one employed in our analysis, which simply eliminates the solar reflex motion. If this is taken into account, we expect the PM results to slightly change, as reported by the authors.

5.1.1 Comparison with Fornax Dwarf Spheroidal Galaxy

The Fornax dSph is one of the closest dwarf galaxies in the Local group to Sagittarius in terms of luminosity. It has $M_v = -13.3$ and a total mass of $M_\odot \approx 1.6 \times 10^8$ (Walker et al., 2006). Nevertheless, this dwarf system is not being disrupted as severely as Sgr. A detailed star formation and chemical evolution history of Fornax is provided in the paper written by de Boer et al., (2012). It is interesting to notice that some findings reported are similar to those achieved for Sgr. Thanks to calibrated photometry and spectroscopic metallicity measurements, the authors demonstrated the existence of a radial gradient of age and metallicity with more metal-rich and younger star forming episodes condensed in the central region. Moving to larger distances from its centre the metallicities shift to lower values and the ages turn older. While the oldest and more MP stars appear at all radii, the younger and MR objects dominate the centre. In our analysis of the metallicity structure of Sgr, we have also discovered a uniform distribution for the VMP selection and found a trend for the MP/MR ratio revealing

an higher relative number of low $[\text{Fe}/\text{H}]$ objects at increasing distances from the centre. Nevertheless, de Boer et al. have extensively employed the SFH method to be able to draw with precision the chemical evolution and history of Fornax and, having available most of the evolutionary features of the galaxy, they could connect the multiple star forming episodes to its metallicity structure.

In our case it was not possible to apply the same method because we do not have the data for all the evolutionary stages for the Sgr sample. Despite this lack, by comparing the MIST isochrones to the Sgr RGB, we have been able to assign an age of $\sim 12 - 13$ Gyr to the VMP sample. This finding does not differ much from the analysis carried out for the Fornax system, whose RGB is dominated by an ancient stellar population with an age ≥ 11 Gyr (de Boer et al., 2012). Besides this similarity, the dominance of an intermediate age SP for both systems indicate that their dynamical masses were sufficient to retain enough gas (before the complete gas loss) to keep forming stars in their inner regions. However, it is important to keep in mind that even if Fornax did experience a gas loss ($> 95\%$, Khalaj & Baumgardt (2016)), it has never fallen so deep into the MW potential as occurred for Sgr about 1 Gyr ago (Tepper-García & Bland-Hawthorn, 2018).

5.2 Limitations of the research

In our research we have delineated and developed a scientific analysis on the metallicity distribution of Sgr dSph. However, the work presents some limitations.

Firstly, due to the small number of spectroscopic data, especially for the most MP stars, we have not been able to study the distribution of the very low $[\text{Fe}/\text{H}]$ objects in detail and with high precision. The PIGS follow-up, which would have been a powerful tool in tracing the VMP stars, is limited in the number of targets and not homogeneous on the Sgr footprint as it has very few data for the less dense regions far from the centre. This implies that its metallicity distribution could be asymmetric and less statistically robust in the search in the outer areas. However, the inhomogeneity of the spectroscopic follow-up is not affecting the “photometric” metallicity distribution as we can rely on the photometric catalogue which does has coverage over the whole footprint, and is very complete for our main results. However, the photometric results are more affected by extinction and its corrections, therefore they are less precise and accurate than any spectroscopic catalogue would be.

On the other hand we saw that the application of the CaT relation requires going through different steps (e.g. the transformation from BP , RP to V band, the assumption of a perfect HB and the use of the corresponding mean magnitude V_{HB}) and might create uncertainties in the derived $[\text{Fe}/\text{H}]$ results, in particular for higher metallicity (see plot 3.18).

The accuracy of the proper motions and contamination of Milky Way stars are additional limitations that concern our work. Nevertheless, these limitations will be hopefully overcome with the arrival of *Gaia* EDR3, which will provide the proper mo-

tion measurements improved by on average a factor 2 with respect to the second data release ¹.

Another important concern that affects our research is the contamination from M54, a problem which has been introduced already in the previous section (5.1). To reduce its effect, we have eliminated some stars at the very centre of Sgr where M54 lies (sect. 3.4.3). This cut may have omitted some objects belonging to the GC which may produce biases in the metallicity analysis of the Sgr system. Nevertheless, this contamination should only affect the very inner-most points in the MP/MR ratio. Hence, the conclusions are not altered and the metallicity distribution does still provide a general picture of the distribution of the Sgr stars in function of their iron content.

A step further in this research would be the comparison between this “small” scale variation in metallicity found in the Sgr remnant with the the kpc-scale gradient observed by many investigations in its spectacular stellar streams (e.g. Chou et al. (2007), Bellazzini et al. (2006), Johnson et al. (2020)). A possible analogy would help to gain a broader insight about the original metallicity distribution of Sgr dSph and its consequent evolution.

Ultimately, regarding the possibility to build an accurate and comprehensive age-metallicity relation for Sgr, it would have been fundamental to have a complete set of data for all the evolutionary stages of the system. In this way, by applying the SFH method, we would have possibly gained a broader insight about the relation between its metallicity and evolution.

Lastly, if in the future it will be possible to get better photometric metallicities, we could look at the Sgr metallicity distribution in more detail and not restrict our analysis to a “simple” division in single MP or MR bins.

5.3 Future outlook

This work has demonstrated that the Pristine metallicity-sensitive narrow-band photometry is a powerful tool to study the metallicity of the Sgr Spheroidal Galaxy. By analysing the metallicity distribution and paying particular attention to the metal-poor population, we prove that a clear metallicity gradient emerges while tracing the relative ratio of MP stars in different parts of the galaxy.

However, to obtain a more comprehensive view of the issue, it would be really meaningful to extend the study of the metallicity distribution to the stellar tails as they are on average 1 dex more MP with respect to the Sgr core (Johnson et al., 2020). Regarding this matter, as part of the CaT dataset there is a fourth sample that covers the Sgr streams (fig. 5.1). With the CaT method and the relation 3.1, it would be possible to calculate the metallicity values for the different parts of the tails using the measurements of the EWs and the looking how the [Fe/H] content varies moving along the streams. A possible difficulty of this operation is the derivation of the distances for the different parts of the tails. Indeed, due to their complex spatial distribution and

¹<https://www.cosmos.esa.int/web/gaia/earlydr3>

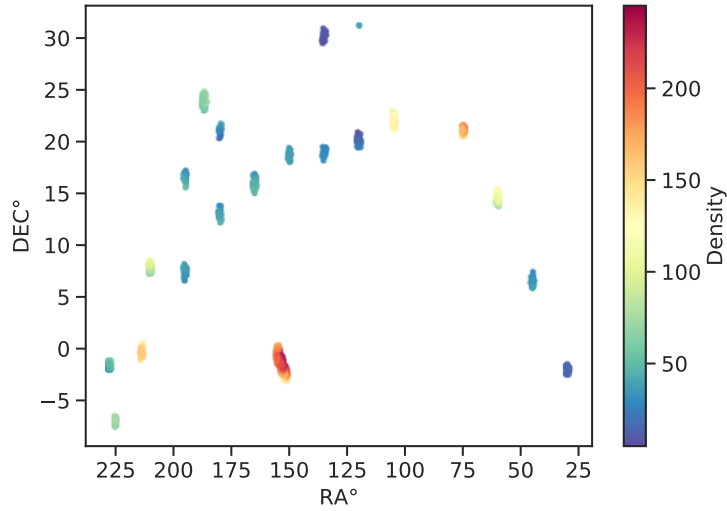


Figure 5.1 – The plot shows data point representing the stellar streams of Sagittarius provided by the CaT catalogues. The colour-coding denotes the stellar density.

their multiple wraps, the mean V magnitude for the horizontal branch (V_{HB} term) is not so trivial to derive. Nevertheless, such analysis may help in getting a more defined picture about the dynamics and early chemical evolution of Sgr.

It would be also very informative deepen the comparison between the metallicity structure of the MP and MR populations with their motions, especially looking at their radial velocities and proper motion dispersion, so to be able to track possible differences in their kinematics.

With respect to the (very) MP stars, to broaden their search a spectroscopic follow-up has been proposed as part of the PIGS program. It aims to reveal the metal-poor bulge candidates using the spectrograph AAT/AAOmega+2dF. A part of the observations is dedicated to Sgr stars. A sample of 400 Sgr stars, already obtained as part of the bulge follow-up, have successfully increased the number of low $[\text{Fe}/\text{H}]$ objects (down to $[\text{Fe}/\text{H}] < -2$) discovered in the dwarf system. In fact, in this work our VMP population consists of about 80 VMP stars with $\langle [\text{Fe}/\text{H}] \rangle \sim -2.16$ and $\sigma \sim 0.34$. This is already a rather larger sample compared to the one presented by Chiti & Frebel (2019), which accounts for 4 metal poor stars with $-2.2 < [\text{Fe}/\text{H}] < -1.6$ or to the 13 VMP red giants with $-3 < [\text{Fe}/\text{H}] < -1$ identified by Hansen et al. (2018). The fields observed as part of the follow-up are located along the major and minor axis in the less dense regions far away from the very centre of Sgr and the magnitude range for the Sgr selection would reach $G < 17$. The research of low metallicity stars in the system will hopefully reveal the EMP and VMP stars that are still undiscovered. The possible detection of these objects would be fundamental in order to have a more precise map of the very low $[\text{Fe}/\text{H}]$ component in Sgr and for enabling a comprehensive study of the metal poor Sgr which is currently lacking due to the low number of MP stars discovered so far.

In addition, collecting more information in the outermost regions would plausibly clarify even more the metallicity gradient spotted in the most central areas and thus provides additional hints about the evolution of the Sgr dwarf system.

Lastly, a crucial point for obtaining a more comprehensive understanding of Sgr is the relation between the age and metallicity of its stars. To this aim, it is highly important to investigate deeper the age models for the Sgr members (e.g. establishing a robust criteria to assess the goodness of the fit for the different isochrone models), and to compare the ages of the Sgr populations showing different metallicities.

Chapter 6

Summary and conclusion

Metal-poor stars are extremely valuable for investigating the conditions of the early Universe. Especially, dwarf galaxies orbiting the Galaxy, which have been shown to host these “archaeological evidences” (Frebel & Norris, 2011; Starkenburg, 2011), constitute unique environments for exploring the history of our local Universe. Among them, we focused our work on the Sagittarius dwarf system, which has been disrupting during the last 2.5 - 3.0 Gyr because of the tidal interaction with the Milky Way. Its special dynamical scenario together with the MP population discovered in the galaxy make it a very compelling target for studying the metallicity distribution (with a special focus on the more MP objects) and for exploring its evolution and influence on the MW halo.

In this thesis, we have studied the Sgr system analysing its metallicity distribution and attempting to highlight the main differences in the distributions of the MP and MR populations. We have used the photometric data from the PIGS survey which combines the narrow-band Ca H&K photometry with the *Gaia* DR2 broadband *G*, *BR* and *RP* photometry. Covering also the Sgr region, PIGS with its metallicity sensitive photometry has permitted to distinguish the MP from the MR population and to select the most MP objects within the Sgr sample. We also employed the spectroscopic information provided by three different catalogues. The APOGEE and the PIGS follow-up metallicity measurements have been combined with the CaT - [Fe/H] results in the colour-colour diagram 4.2 to better appreciate the metallicity spread in the Sgr colour space. At that point, it has been possible cutting the photometric sample into two metallicity populations and later isolate the VMP components. Furthermore, by applying the CaT calibration formula (3.1) on the Sgr stars we were able to test the validity of the above-mentioned relation for a dwarf galaxy. We found good agreement in the results, especially in the lower metallicity regime.

The spectroscopic metallicities have been further employed to compute the average metallicity and dispersion for the “photometric” MP ($\langle [\text{Fe}/\text{H}] \rangle \sim -1.64 \pm 0.27$) and MR ($\langle [\text{Fe}/\text{H}] \rangle \sim -0.53 \pm 0.20$) groups. By plotting their spatial distributions (graph 4.3), it is immediately visible that the stellar density for both samples is higher around

the centre of Sgr, where M54 lies. This feature affects our metallicity study as the irregular stellar density impedes to have statistically robust results for the outermost Sgr regions. Nevertheless, to have a deeper insight in the metallicity content of our Sgr selection, we divided it in different ways to examine the variation of the MP/MR ratio moving in space within the Sgr footprint. From this analysis it resulted that the relative fraction of MP stars seems to rise with the increasing distance from the very centre of Sgr, which coincides with the position of the GC M54. Being aware of the inhomogeneous coverage and of the possible contamination from the GC, we compared this outcome with studies covering the same topic finding that a metallicity gradient has been widely recognised in Sgr galaxy. It does suggest a more MR component (excluding the metal-poor contribution of M54) dominating the central part and an increasing relative fraction of MP stars at the outskirts of the dwarf. This leads us to suppose that the MP component has been the first to be formed, and the first to be stripped away and distributed along the tidal tails and to the Milky Way Galactic halo.

Attempting to have a greater understanding about the metallicity structure of Sgr, we have then dedicated a part of the work to study the proper motion of its components. This investigation have brought to the conclusion that the MP and MR stars do not show big variations in their internal motions and structures. The alignment between the overall PM and the elongation of the body found for both populations lead us to confirm that the Sgr stars, following the orbit direction, are gradually removed from the nucleus and transferred into the two tidal streams.

Digging deeper into the matter, we have focused on the link between the metallicity structure and the history of Sgr examining the age of the VMP component. By employing models for isochrones based on the *Gaia* photometry, we reach the conclusion that the VMPs have an age about 12-13 Gyr. Hence, they are part of an old and metal-poor stellar population hosted by the galaxy. Analysing their distribution, we found out that they are homogeneously spread and not centrally peaked, a feature which is also shared by the more metal poor stars. Indeed, the transition between a clearly peaked distribution and a more flat distribution occurs at $[\text{Fe}/\text{H}] \sim -1.68$ which corresponds to a cut at $y = 6$ in the Sgr CCD. Objects laying below this value are uniformly distributed along the main body of the dwarf. Bringing together these results we are led to think that the metal poor component of the galaxy have been well mixed with different metallicity-groups. We suppose that Sgr dSph encountered during its existence metal rich star bursts occurring only at the very centre of the galaxy. This may also be the reason behind the metallicity gradient revealed in the system.

In conclusion, the metallicity analysis performed with the different tools and techniques presented in this thesis can pave the way for an intriguing discussion about the relation between the metallicity distribution of the galaxy, its formation, evolution and star formation history. Indeed, with its history of tidal disruption, this dwarf galaxy is also a rare workshop for examining the physical aspects connected to the metallicity and chemical evolution from the perspective of the hierarchical galaxy formation scenario.

Chapter 7

Bibliography

- Aguado D. S., Hernández J. I. G., Prieto C. A., Rebolo R., 2019, *The Astrophysical Journal Letters*, 874, L21
- Alfaro-Cuello M., et al., 2019, *The Astrophysical Journal*, 886, 57
- Arentsen A., et al., 2020, arXiv preprint arXiv:2006.08641
- Armandroff T. E., Da Costa G., 1991, *The Astronomical Journal*, 101, 1329
- Armandroff T. E., Zinn R., 1988, *The Astronomical Journal*, 96, 92
- Battaglia G., Irwin M., Tolstoy E., Hill V., Helmi A., Letarte B., Jablonka P., 2008, *Monthly Notices of the Royal Astronomical Society*, 383, 183
- Beers T. C., Christlieb N., 2005, *Annu. Rev. Astron. Astrophys.*, 43, 531
- Bellazzini M., Ferraro F., Buonanno R., 1998, arXiv preprint astro-ph/9812344
- Bellazzini M., Ferraro F., Buonanno R., 1999, *Monthly Notices of the Royal Astronomical Society*, 307, 619
- Bellazzini M., Newberg H., Correnti M., Ferraro F., Monaco L., 2006, *Astronomy & Astrophysics*, 457, L21
- Bellazzini M., et al., 2008, *The Astronomical Journal*, 136, 1147
- Belokurov V., et al., 2014, *Monthly Notices of the Royal Astronomical Society*, 437, 116
- Bessell M., Norris J., 1984, *The Astrophysical Journal*, 285, 622
- Bromm V., 2013, *Reports on Progress in Physics*, 76, 112901
- Carretta E., Bragaglia A., Gratton R., D’Orazi V., Lucatello S., 2009, *Astronomy & Astrophysics*, 508, 695
- Carretta E., et al., 2010, *Astronomy & Astrophysics*, 520, A95

- Chiti A., Frebel A., 2019, *The Astrophysical Journal*, 875, 112
- Chou M.-Y., et al., 2007, *The Astrophysical Journal*, 670, 346
- Christlieb N., Schörck T., Frebel A., Beers T., Wisotzki L., Reimers D., 2008, *Astronomy & Astrophysics*, 484, 721
- D’Onghia E., Lake G., 2008, *Proceedings of the International Astronomical Union*, 4, 473
- DR2 G., , Gaia DR2 Main table, <https://gea.esac.esa.int/archive/documentation/GDR2/>
- Da Costa G., Armandroff T., 1995, *The Astronomical Journal*, 109, 2533
- De Boer K., 2012, *Stars & Stellar evolution. EDP sciences*, pp 217–220
- De Lucia G., Helmi A., 2008, *Monthly Notices of the Royal Astronomical Society*, 391, 14
- Dotter A., 2016, *The Astrophysical Journal Supplement Series*, 222, 8
- Evans D., et al., 2018, *Astronomy & Astrophysics*, 616, A4
- Ferguson P. S., Strigari L. E., 2020, *Monthly Notices of the Royal Astronomical Society*, 495, 4124
- Frebel A., Norris J. E., 2011, arXiv preprint arXiv:1102.1748
- Freeman K., 1993, in *The Globular Cluster-Galaxy Connection*. p. 608
- Fritz T., Battaglia G., Pawlowski M., Kallivayalil N., Van Der Marel R., Sohn S., Brook C., Besla G., 2018, *Astronomy & Astrophysics*, 619, A103
- Gaia C., et al., 2018, *Astronomy & Astrophysics*, 616
- Hansen C. J., El-Souri M., Monaco L., Villanova S., Bonifacio P., Caffau E., Sbordone L., 2018, *The Astrophysical Journal*, 855, 83
- Harris W. E., , Catalogue of parameters of Milky Way Globular Clusters, <http://physwww.mcmaster.ca/~harris/mwgc.dat>
- Harris W. E., 2010, arXiv preprint arXiv:1012.3224
- Hartwick F., 1976, *The Astrophysical Journal*, 209, 418
- Hasselquist S., et al., 2017, *The Astrophysical Journal*, 845, 162
- Helmi A., et al., 2006, *The Astrophysical Journal Letters*, 651, L121
- Helmi A., et al., 2018, *Astronomy & Astrophysics*, 616, A12
- Ibata R., 1999, in *Symposium-International Astronomical Union*. pp 39–46

- Ibata R., Gilmore G., Irwin M., 1994, *Nature*, 370, 194
- Ibata R., Wyse R., Gilmore G., Irwin M., Suntzeff N., 1996, arXiv preprint astro-ph/9612025
- Ibata R., Lewis G. F., Irwin M., Totten E., Quinn T., 2001, *The Astrophysical Journal*, 551, 294
- Johnson B. D., et al., 2020, arXiv preprint arXiv:2007.14408
- Keller S., et al., 2014, *Nature*, 506, 463
- Khalaj P., Baumgardt H., 2016, *Monthly Notices of the Royal Astronomical Society*, 457, 479
- Koposov S. E., et al., 2012, *The Astrophysical Journal*, 750, 80
- Kurucz R., Barbuy B., Renzini A., 1992, in *IAU symp.* p. 225
- Law Majewski, Simulation, <https://faculty.virginia.edu/srm4n/Sgr/data.html>
- Lindgren L., et al., 2018, *Astronomy & Astrophysics*, 616, A2
- Mackey A. D., Gilmore G., 2003, *Monthly Notices of the Royal Astronomical Society*, 340, 175
- Majewski S. R., Skrutskie M., Weinberg M. D., Ostheimer J. C., 2003, *The Astrophysical Journal*, 599, 1082
- McConnachie A. W., 2012, *The Astronomical Journal*, 144, 4
- McWilliam A., Wallerstein G., Mottini M., 2013, arXiv preprint arXiv:1309.2974
- Monaco L., Bellazzini M., Ferraro F. R., Pancino E., 2003, *The Astrophysical Journal Letters*, 597, L25
- Mucciarelli A., Bellazzini M., Ibata R., Romano D., Chapman S., Monaco L., 2017, *Astronomy & Astrophysics*, 605, A46
- Müller O., et al., 2020, arXiv preprint arXiv:2011.04990
- Newberg H. J., Carlin J. L., 2015, *Tidal Streams in the Local Group and Beyond*. Springer
- Nordlander T., Amarsi A. M., Lind K., Asplund M., Barklem P. S., Casey A. R., Collet R., Leenaarts J., 2017, *Astronomy & Astrophysics*, 597, A6
- Price-Whelan A. M., 2017, *The Journal of Open Source Software*, 2
- Prieto C. A., Beers T. C., Wilhelm R., Newberg H. J., Rockosi C. M., Yanny B., Lee Y. S., 2006, *The Astrophysical Journal*, 636, 804

- Qiu H.-M., Zhao G., Takada-Hidai M., Chen Y.-Q., Takeda Y., Noguchi K., Sadakane K., Aoki W., 2002, *Publications of the Astronomical Society of Japan*, 54, 103
- Ruiz-Lara T., Gallart C., Bernard E. J., Cassisi S., 2020, arXiv preprint arXiv:2003.12577
- Sarajedini A., Layden A. C., 1995, *The Astronomical Journal*, 109, 1086
- Sbordone L., Hansen C., Monaco L., Cristallo S., Bonifacio P., Caffau E., Villanova S., Amigo P., 2020, arXiv preprint arXiv:2005.03027
- Schlegel D. J., Finkbeiner D. P., Davis M., 1998, *The Astrophysical Journal*, 500, 525
- Schörck T., et al., 2009, *Astronomy & Astrophysics*, 507, 817
- Sagittarius Dwarf to Collide with Milky Way, <https://apod.nasa.gov/apod/ap980216.html>
- Siegel M. H., et al., 2007, *The Astrophysical Journal Letters*, 667, L57
- Simbad, SIMBAD Astronomical Database - CDS (Strasbourg), <http://simbad.u-strasbg.fr/simbad/>
- Starkenburger E., 2011, *Galactic archaeology in and around the Milky Way*
- Starkenburger E., et al., 2010, *Astronomy & Astrophysics*, 513, A34
- Starkenburger E., et al., 2017, *Monthly Notices of the Royal Astronomical Society*, 471, 2587
- Tepper-García T., Bland-Hawthorn J., 2018, *Monthly Notices of the Royal Astronomical Society*, 478, 5263
- Tolstoy E., Hill V., Tosi M., 2009, *Annual Review of Astronomy and Astrophysics*, 47, 371
- Tremonti C. A., et al., 2004, *The Astrophysical Journal*, 613, 898
- Vasiliev E., Belokurov V., 2020, arXiv preprint arXiv:2006.02929
- Vasiliev E., Belokurov V., Erkal D., 2020, arXiv preprint arXiv:2009.10726
- Velázquez H., White S. D., 1995, *Monthly Notices of the Royal Astronomical Society*, 275, L23
- Walker M. G., Mateo M., Olszewski E. W., Bernstein R., Wang X., Woodroffe M., 2006, *The Astronomical Journal*, 131, 2114
- Wenger M., et al., 2000, *Astronomy and Astrophysics Supplement Series*, 143, 9
- Youakim K., et al., 2017, *Monthly Notices of the Royal Astronomical Society*, 472, 2963

CHAPTER 7. BIBLIOGRAPHY

Youakim K., et al., 2020, Monthly Notices of the Royal Astronomical Society, 492, 4986

de Boer T., et al., 2012, Astronomy & Astrophysics, 544, A73

del Pino A., Fardal M. A., van der Marel R. P., Lokas E. L., Mateu C., Sohn S. T., 2020, arXiv preprint arXiv:2011.02627

for Survey H. A. C., , Messier M54, <https://spacetelescope.org/images/potw1145a/>

Appendices

Appendix A

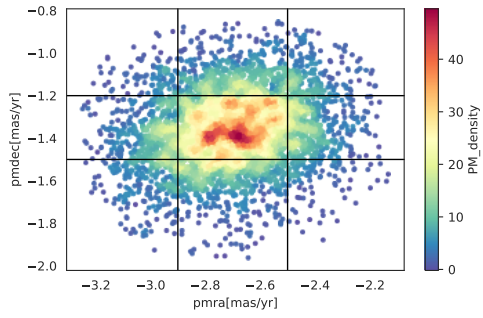
Here we report the plots of the PM space for the star samples selected for each annulus (see the concentric division reported in sec. 4.2.1). Each single plot is referred to a ring. The colour-coding provides the stellar density, and in the captions it is reported for each ring the corresponding equatorial distance range in degrees.

For the first five graphs it is noticeable that the main over-density remains in the central square, while for the last annuli the central over-density moves across the equatorial coordinates and exits the central box. These charts reinforce the idea that the proper motion selection designed for the very inner region is no longer valid for the outer stellar components. This can be explained by referring to the variation in PM across the Sgr body indicated by Vasiliev & Belokurov and already explained in section 4.1.1. Nevertheless, if we simply try to change the PM selection by tracking the movement in PM space of the central over-density the results do not improve much as it evidenced by the figure A.1.

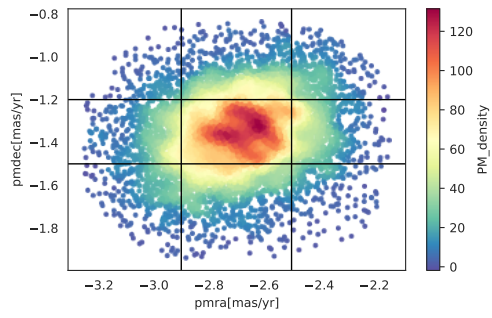
To try to mitigate the effects of the bad statistics of the outermost rings, we try to sum the four last annuli and then to apply the PM correction on this new group of data. Albeit this modification does not influence the trend for the outer stars, it improves the error bar on this sum of data, as the the number of stars that fall into this new division is now grater compared to the previous one, see fig A.2.

We can therefore conclude that more complex corrections are necessary to consider the PM variation along the body of Sgr and a deeper comprehension of the kinematics of the Sgr stars is necessary to be able to define a more solid selection for the external region of the system.

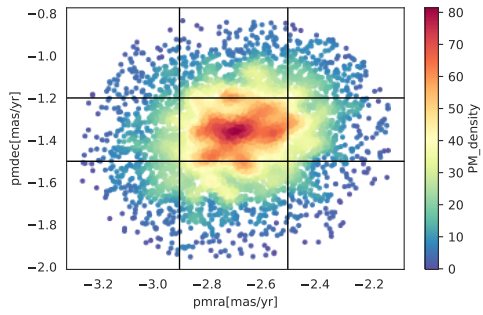
APPENDIX A.



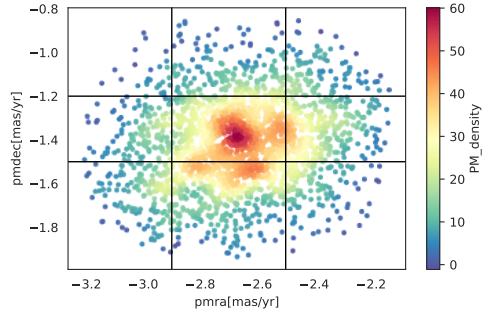
(a) $0^\circ < y < 1.5^\circ$



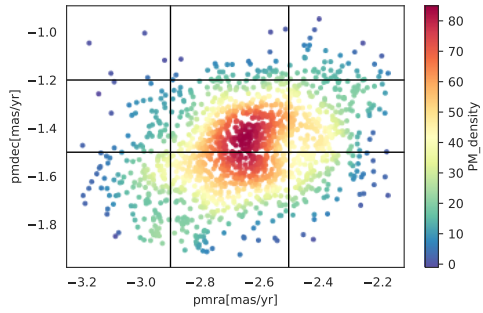
(b) $1.5^\circ < y < 3^\circ$



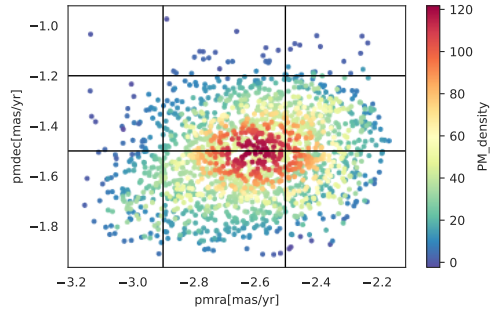
(a) $3^\circ < y < 4.5^\circ$



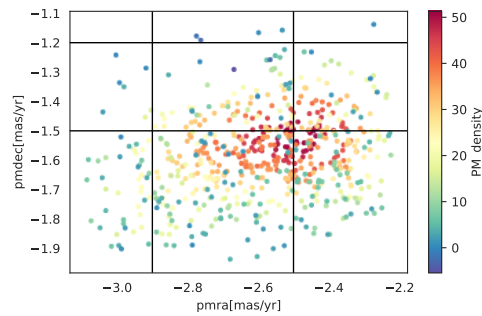
(b) $4.5^\circ < y < 6^\circ$



(a) $6^\circ < y < 7.5^\circ$



(b) $7.5^\circ < y < 10.5^\circ$



(c) $10.5^\circ < y < 16.5^\circ$

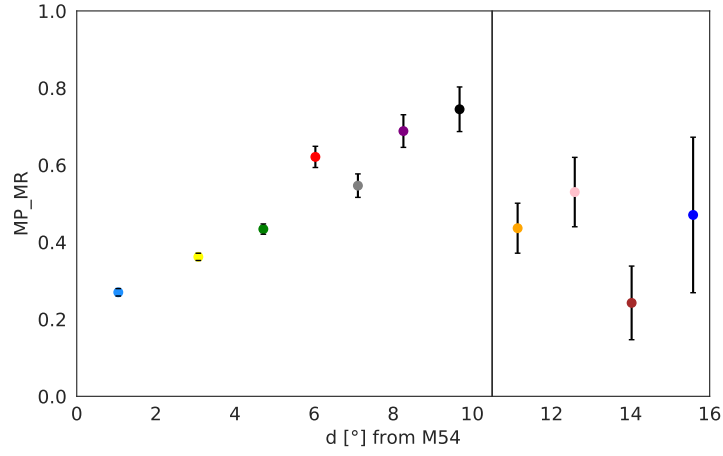


Figure A.1 – The ratios of MP/MR stars calculated for each annulus. The x-axis represents the distances from the position of M54. The black vertical line separate the last annuli for which the PM condition has been changed.

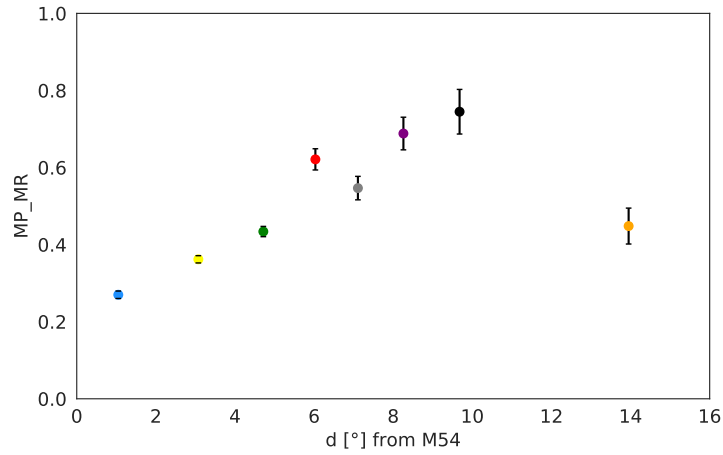
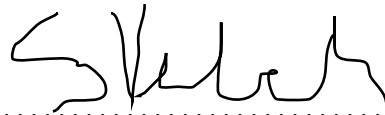


Figure A.2 – The ratios of MP/MR stars calculated for each annulus. The x-axis represents the rings. In this case the last data point, represented by the orange dot, is the sum of the four last annuli (the ones located on the right of the black vertical line in the plot A.1) on which we have applied the corrections for the PM. The corresponding error bars is reduced as now the number of stars enclosed in this sum is considerably higher compared to the previous distribution.

Statement of Originality

I hereby declare that this thesis is the product of my own work. All the assistance received in preparing this thesis and the sources used have been acknowledged.

Potsdam, 11/12/2020

A handwritten signature in black ink, consisting of several stylized, connected letters, positioned above a horizontal dotted line.

(Signature of the candidate)

Acknowledgements

It's a strange feeling to be at the end of a project, a work that you realize meaning so much for you. Now, in such a strange period, made of gaps and long reflections, the awareness of having completed my thesis seems to me almost unrealistic. Despite this, going through this thesis again gives me a deep sense of satisfaction. Between its lines I see all the effort put into by the people involved. For this, I want to thank you my supervisors, Else and Anke, who welcomed me into their team, allowing me to learn new things and to approach interesting topics. They have kindly opened to me an unknown and fascinating world. Thanks for your patience and trust.

Thanks to all the people from the AIP with who I have collaborated in these months. I have found a special environment which have offered me many possibilities and where I had the chance to learn more. Gracias querida Silke, tú que cada mañana tenía una sonrisa para mi, con lluvia o sol.

Grazie ai miei genitori, a Neri, che con le loro telefonate (o quelle mancate) non hanno mai smesso di farmi sentire a casa e non mi hanno fatto mai mancare nulla. Grazie anche te che mi guardi sempre dalla mia scrivania e che saresti stata la prima a voler leggere il mio lavoro.

Grazie a te Gio, per avermi dato la tua amicizia, così viva e chiara da aver vinto tutte le distanze. Grazie a Robi per le risate strappate durante le telefonate, grazie a tutti gli amici che mi hanno ascoltata, resa partecipe della loro vita in modo da non farmi sentire mai troppo sola. Elsa, tu che sei stata qui di fianco, con i tuoi sforzi che hanno dato più senso ai miei, con il tuo sguardo che ha sempre capito cosa avevo per la testa, sei stata e sei ormai necessaria. Grazie a Paolo che ha condiviso con me la sua preziosa esperienza e utili consigli e che mi ha fatto vivere in modo diverso questa grande città. Grazie alle persone che ho incontrato a Berlino e che mi hanno permesso di costruire delle cose di cui avrò sempre preziosi ricordi.

Gracias a tí que siempre estás a mi lado, no importa las condiciones y que siempre has creído en esto.